The binding mechanism of the virulence factor *Streptococcus suis* adhesin P subtype to globotetraosylceramide is associated with systemic disease

Received for publication, June 16, 2020, and in revised form, August 11, 2020 Published, Papers in Press, August 12, 2020, DOI 10.1074/jbc.RA120.014818

Miralda Madar Johansson[1,‡], Eva Bélurier[2,‡], Anastassios C. Papageorgiou[3], Anders P. Sundin[4], Jani Rahkila[5], Teemu Kallonen[6,7,8], Ulf J. Nilsson[4], Santeri Maatsola[2], Thomas K. M. Nyholm[9], Jarmo Käpylä[10], Jukka Corander[6,8,11], Reko Leino[12], Jukka Finne[13], Susann Teneberg[1], and Sauli Haataja[2,*]

From the [1]Department of Medical Biochemistry and Cell Biology, Institute of Biomedicine, Sahlgrenska Academy at University of Gothenburg, Gothenburg, Sweden, the [2]Institute of Biomedicine, Research Center for Cancer, Infections and Immunity, University of Turku, Turku, Finland, the [3]Turku Bioscience Centre, University of Turku and Åbo Akademi University, Tykistökatu 6, Turku, Finland, the [4]Centre for Analysis and Synthesis, Department of Chemistry, Lund University, Lund, Sweden, the [5]Instrument Centre, Åbo Akademi University, Turku, Finland, the [6]Department of Biostatistics, University of Oslo, Blindern, Norway, the [7]Department of Clinical Microbiology, Turku University Hospital, Turku, Finland, the [8]Parasites and Microbes, Wellcome Sanger Institute, Cambridge, United Kingdom, the [9]Biochemistry Faculty of Science and Engineering, Åbo Akademi University, Turku, Finland, the [10]Department of Biochemistry, University of Turku, Turku, Finland, the [11]Helsinki Institute for Information Technology (HIIT), Department of Mathematics and Statistics, University of Helsinki, Finland, the [12]Laboratory of Molecular Science and Technology, Åbo Akademi University, Turku, Finland, and the [13]Molecular and Integrative Biosciences Research Programme, Faculty of Biological and Environmental Sciences, University of Helsinki, Helsinki, Finland

Edited by Gerald W. Hart

Streptococcus suis **is part of the pig commensal microbiome but strains can also be pathogenic, causing pneumonia and meningitis in pigs as well as zoonotic meningitis. According to genomic analysis, *S. suis* is divided into asymptomatic carriage, respiratory and systemic strains with distinct genomic signatures. Because the strategies to target pathogenic *S. suis* are limited, new therapeutic approaches are needed. The virulence factor *S. suis* adhesin P (SadP) recognizes the galabiose Galα1–4Gal-oligosaccharide. Based on its oligosaccharide fine specificity, SadP can be divided into subtypes P_N and P_O. We show here that subtype P_N is distributed in the systemic strains causing meningitis, whereas type P_O is found in asymptomatic carriage and respiratory strains. Both types of SadP are shown to predominantly bind to pig lung globotriaosylceramide (Gb3). However, SadP adhesin from systemic subtype P_N strains also binds to globotetraosylceramide (Gb4). Mutagenesis studies of the galabiose-binding domain of type P_N SadP adhesin showed that the amino acid asparagine 285, which is replaced by an aspartate residue in type P_O SadP, was required for binding to Gb4 and, strikingly, was also required for interaction with the glycomimetic inhibitor phenylurea-galabiose. Molecular dynamics simulations provided insight into the role of Asn-285 for Gb4 and phenylurea-galabiose binding, suggesting additional hydrogen bonding to terminal GalNAc of Gb4 and the urea group. Thus, the Asn-285–mediated molecular mechanism of type P_N SadP binding to Gb4 could be used to selectively target *S. suis* in systemic disease without interfering with commensal strains, opening up new avenues for interventional strategies against this pathogen.**

Bacterial adhesion to host cell surfaces is a prerequisite for infectious disease. Host cell surfaces are heavily covered by surface carbohydrates that form the glycocalyx layer (1, 2). Pathogenic bacteria and their toxins can treacherously exploit carbohydrates to attach and invade cells. One example is a group of endogenous glycosphingolipids, known as globo series membrane glycosphingolipids, which are grouped based on the Galα1–4Gal (galabiose) structure. Globo series glycolipids are cellular receptors for toxic action of Verotoxins and for the attachment of bacteria, such as uropathogenic *Escherichia coli*, *Streptococcus suis*, and *Pseudomonas aeruginosa* (3–6).

Because antibiotics are increasingly losing their power, alternative antimicrobial compounds need to be invented and developed (7, 8). Transformation of bacteria to antibiotic-resistant forms can be overcome by developing compounds that block *in vivo* colonization and virulence factors without killing the pathogens. Cell surface carbohydrate glycomimetics are the most tempting pipeline for the development of new generation of antimicrobials (9, 10).

S. suis is found as a commensal bacterium in all pigs and it is an important pig pathogen causing septicemia, pneumonia, and meningitis. It also causes severe zoonotic meningitis. Based on clinical outcome, the *S. suis* strains can be classified as asymptomatic carriage, respiratory, and systemic strains. Recent data show that *S. suis* produces an alarmingly vast array of factors causing high antibiotic resistance (11). Genomic analysis shows that the asymptomatic carriage and systemic strains have clear differences in their core and accessory genomes,

This article contains supporting information.

‡These authors contributed equally to this work.

*For correspondence: Sauli Haataja, sauli.haataja@utu.fi.

Present address for Eva Bélurier: Faculté des Sciences et Technologies (Sciences and Technology Faculty), University of Lille, Lille, France.

whereas respiratory strains have more overlapping features (12). This could suggest that environmental factors such as overcrowding and synergistic activities with other keystone pathogens (13) can alter pigs to develop severe symptoms and pneumonia. Instead, the virulence genes are enriched in systemic strains and their accessory genomes contribute to the invasive *S. suis* infections and meningitis (12). There is multiple and redundant colonization and virulence factors required for *S. suis* disease. The distribution of virulence factors is also different depending on the geographical regions impacting the accessory genomes, which hampers the development of effective vaccines (14). To develop new therapeutics and vaccines the molecular mechanisms of accessory virulence factors need to be resolved in atomic level.

S. suis strains expressing SadP adhesin bind specifically to Galα1–4Gal-containing oligosaccharides (15). Interestingly, galabiose-binding strains can be divided to subtypes P_N and P_O based on how they recognize galabiose-containing carbohydrates in hemagglutination assays (16). Type P_N strains recognize galactose, *N*-acetylgalactosamine, and the ceramide-linked oligosaccharides Gb3 (Galα1–4Galβ1–4Glc) and Gb4 (GalNAcβ1–3Galα1–4Galβ1–4Glc). Subtype P_O recognizes only galactose and preferentially binds to Gb3. Recently, *S. suis* galabiose-binding adhesin SadP was identified as an LPNTG-anchored cell-wall protein (6). The carbohydrate interaction of SadP has been shown to mediate *S. suis* binding to pharyngeal epithelium and intestinal epithelial cells (16, 17). In an *S. suis* murine infection model, the mice deficient in globotriaosyl ceramide (Gb3) expression (knockout in α-1,4-galactosyltransferase A4GALT) developed less severe brain inflammation and injury (18). Recently, low picomolar concentrations of glycomimetic 3-phenylurea-galabiose–containing dendrimers were shown to block *S. suis* SadP (type P_N) adhesion-binding activity (19). However, the molecular basis of differences in galabiose-binding mechanisms of SadP adhesins have remained elusive. In the present study, we have characterized the distribution of SadP subtypes in *S. suis* strains and the molecular binding mechanism of type P_N and P_O SadP to globosyl oligosaccharides. The results show that *S. suis* SadP-type P_N is distributed in the systemic strains and its specific Asn-285–mediated binding mechanisms to globotetraosyl ceramide distinguishes it from type P_O sadP.

Results

Sequence analysis of SadP subtypes P_N and P_O, structural modeling, and distribution in S. suis systemic, respiratory, and nonclinical strains

SadP adhesins are 80-kDa LPNTG-anchored cell-wall proteins, which contain the signal sequence for secretion, the N-terminal galabiose-binding domain, tandem repeat domains, and C-terminal LPNTG cell-wall anchor domain (6). The galabiose-binding domains have no significant sequence homologs to other bacterial proteins or to other carbohydrate-binding domains. The SadP N-terminal galabiose-binding domains (aa 31-328) of hemagglutinating type P_N and type P_O strains were cloned, sequenced, and compared with multiple sequence alignment (Fig. 1*A*). The structure consists of three α-helices and 10 β-strands (β1-β10) that form a β-sandwich core domain. The sequences of the N-terminal galabiose-binding domain of type P_N SadP adhesins are 100% identical and are found in virulent serotype 2 strains. There is more sequence variation in the galabiose-binding site of type P_O SadP. The carbohydrate-binding sites of types P_N and P_O are highly conserved (Fig. 1*A*). Interestingly there is a conservative change at position 285 from asparagine to aspartate, which could have an effect for the interaction of type P_N SadP with GalNAcβ1–3Galα1–4Gal-oligosaccharide.

The distribution of *sadP* genes in clinical and nonclinical strains analyzed with core genome phylogeny analysis is shown in Fig. 1*B*. The gene of *sadP*-type P_N was found in 91.9% of systemic *S. suis* isolates (88.1% of strains isolated from brain), whereas only less than 1% of strains had the gene encoding *sadP*-type P_O. Based on the maximum-likelihood core genome phylogeny analysis the type P_N SadP gene is found in clonal virulent *S. suis* strains, which mostly belong to serotype 2. Interestingly, also serotype 14 strains isolated from human meningitis cases have the type P_N gene. Type P_O *sadP* was found more frequently in respiratory and nonclinical strains.

For the studies comparing the glycosphingolipid binding specificity of WT SadP type P_N and P_O adhesins, the N-terminal region (aa 31-328) containing the galabiose-binding domain were cloned to pET46 vector for production of recombinant proteins as described under "Experimental procedures." For the site-specific mutagenesis, crystal structure, and STD-NMR studies, only the galabiose-binding domain (aa 125-329) of type P_N SadP was used.

Purification and analysis of glycosphingolipid composition of porcine lung

The interaction of recombinant SadP with globo series glycolipids has not been thoroughly characterized. Moreover, whether SadP binds to Gb3 or Gb4 isolated from the pig tissues has not yet been directly shown. The glycolipids were isolated from porcine lung and erythrocytes, to control that the glycolipids isolated from the lungs were not contaminants derived from the erythrocytes remaining in the lungs. The total nonacid glycosphingolipid fractions were hydrolyzed with endoglycoceramidase II of *Rhodococcus* sp., and the oligosaccharides thereby obtained were analyzed by LC-ESI/MS using graphitized carbon columns. This method gives resolution of isomeric oligosaccharides, and the MS^2 analyses gives complete sequence information and allows differentiation of linkage positions by diagnostic cross-ring ^{0,2}A-type fragment ions (20).

The base peak chromatograms from LC-ESI/MS of the oligosaccharides obtained by hydrolysis of the total nonacid glycosphingolipid fractions of porcine erythrocytes and lung were determined (Fig. 2*A*). By comparison of the retention times and MS^2 spectra of oligosaccharides obtained from reference glycosphingolipids, the major oligosaccharides obtained from porcine lung were tentatively identified as globotriaosylceramide (Gb3, detected as a $[M\text{-}H^+]^-$ ion at *m/z* 503), the blood group H type 2 pentasaccharide (H5-2, detected as a $[M\text{-}H^+]^-$ ion at *m/z* 852) and the B5/Galili pentasaccharide (B5, detected as a $[M\text{-}H^+]^-$ ion at *m/z* 868) (Fig. 2*A*). The major oligosaccharides from porcine erythrocytes were globotriaosylceramide (Gb3,

detected as a $[M\text{-}H^+]^-$ ion at *m/z* 503), globotetraosylceramide (Gb4, detected as a $[M\text{-}H^+]^-$ ion at *m/z* 706), and the blood group A type 2 hexasaccharide (A6–2, detected as a $[M\text{-}H^+]^-$ ion at *m/z* 1055) (Fig. 2*B*). Thus, globotriaosylceramide was found in both samples, but otherwise the two samples were significantly different. The total nonacid glycosphingolipid

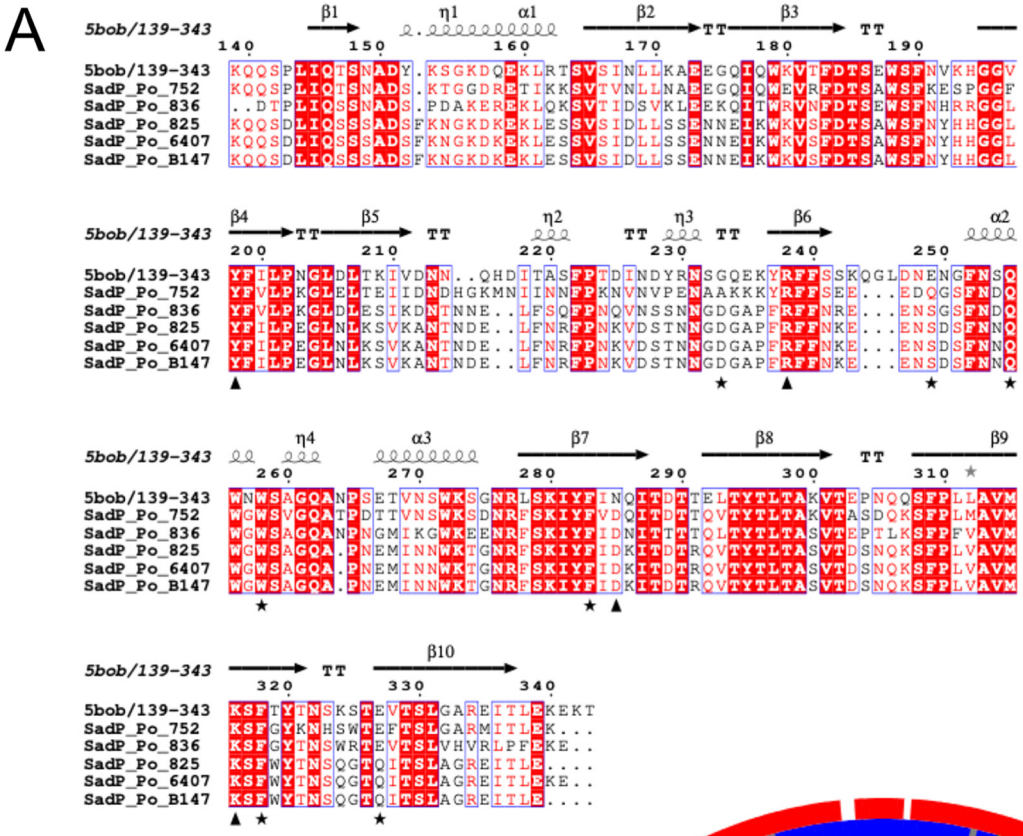

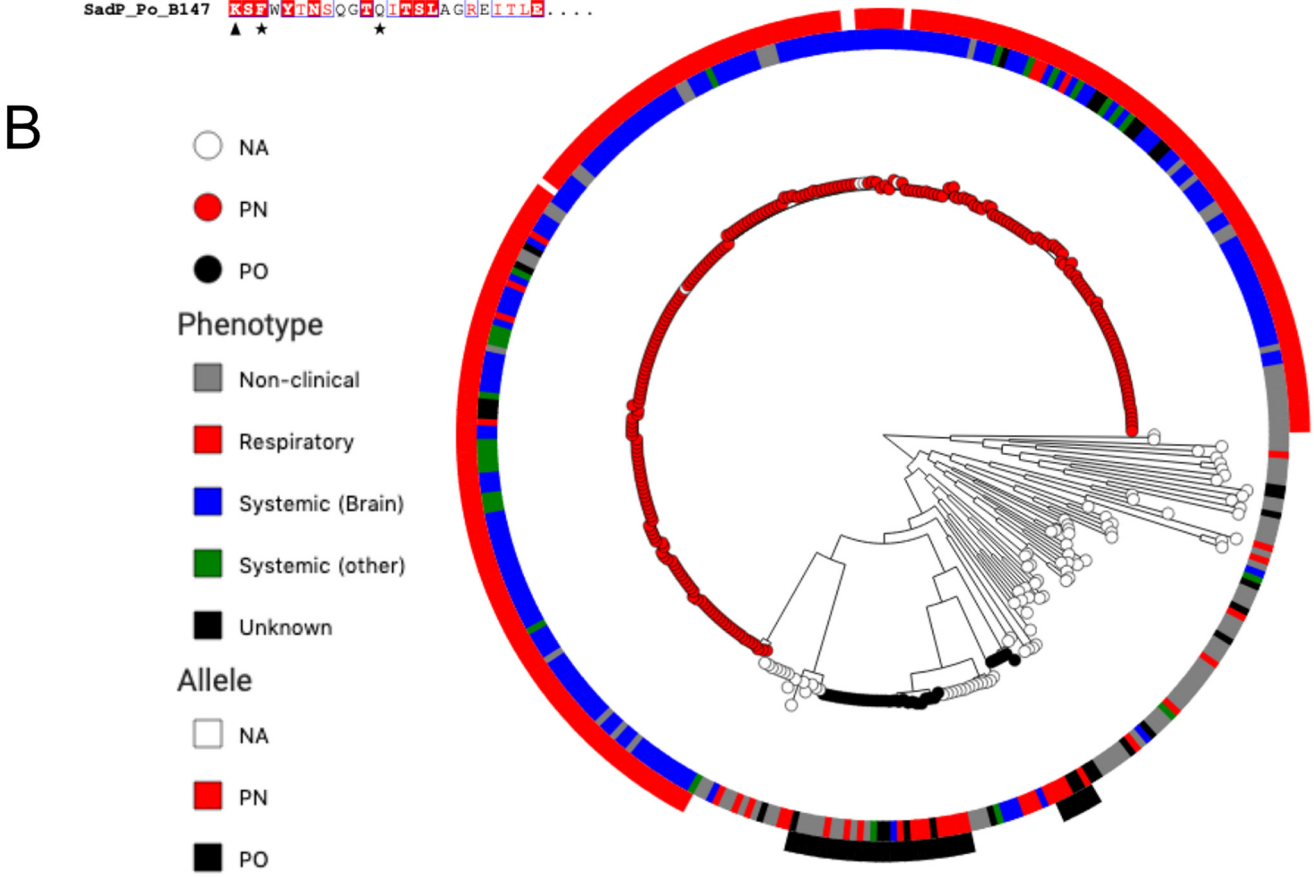

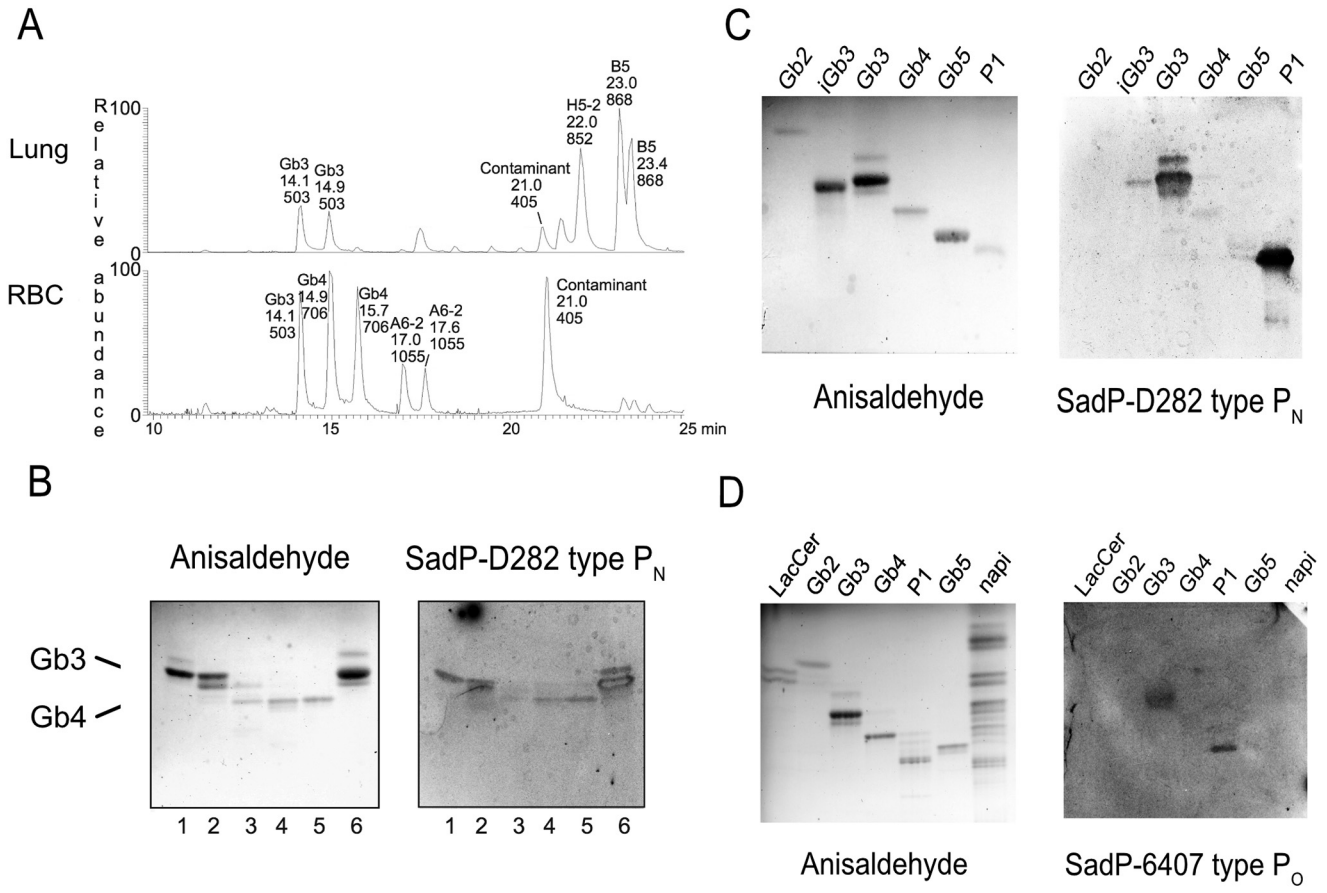

Figure 2. Different glycolipid binding specificities of SadP-type P_N from systemic *S. suis* strains and type P_O SadP from respiratory strains toward pig lung glycolipids and purified globo series glycolipids. *A*, comparison of the total nonacid glycosphingolipid fractions from porcine lung and erythrocytes. Base peak chromatogram from LC-ESI/MS of the oligosaccharides derived the total nonacid glycosphingolipid fraction from porcine lung by digestion with *Rhodococcus* endoglycoceramidase II. *B,* base peak chromatogram from LC-ESI/MS of the oligosaccharides derived the total nonacid glycosphingolipid fraction from porcine erythrocytes by digestion with *Rhodococcus* endoglycoceramidase II. The identification of individual glycosphingolipid-derived oligosaccharides was based on their determined molecular masses and subsequent MS^2 sequencing. The oligosaccharides identified in the chromatograms are: *Gb3*, Galα1–4Galβ1–4Glc; *H5-2*, Fucα2–3Galβ1–4GlcNAcβ1–3Galβ1–4Glc; *B5*, Galα1–3Galβ1–4GlcNAcβ1–3Galβ1–4Glc; *Gb4*, GalNAcβ1–3Galα1–4Galβ1–4Glc; *A6-2*, GalNAcα1–3(Fucα2–3)Galβ1–4GlcNAcβ1–3Galβ1–4Glc. *B*, SadP binding tri- and tetraglycosylceramides isolated from porcine lung. Thin-layer chromatogram after detection with anisaldehyde (*A*), and autoradiograms obtained by binding of SadP (*B*), followed by autoradiography for 12 h, as described under "Experimental procedures." The solvent system used was chloroform/methanol/water (60:35:8, by volume). The lanes were: *lane 1*, fraction PL-1 isolated from pig lung, 1 μg; *lane 2*, fraction PL-2 isolated from pig lung, 1 μg; *lane 3*, fraction PL-3 isolated from pig lung, 1 μg; *lane 4*, fraction PL-4 isolated from pig lung, 1 μg; *lane 5*, reference globotetraosylceramide (GalNAcβ1–3Galα1–4Galβ1–4Glcβ1Cer), 2 μg; *lane 6*, reference globotriaosylceramide (Galα1–4Galβ1–4Glcβ1Cer), 2 μg. *C*, TLC overlay assay with purified glycolipids, SadP-D282 type P_N. *Gb2*, galabiaosylceramide, 2 μg; *iGb3*, isoglotriosylceramide, 4 μg; *Gb3*, globotriosylceramide, 4 μg; *Gb4*, globotetraosylceramide, 4 μg; *Gb5*, Forssman, 4 μg; *P1*, pentaosylceramide, 4 μg. *D,* SadP-6407 type P_O. Lactosylceramide, 4 μg; galabiaosylceramide, 4 μg; globotriaosylceramide, 4 μg; globotetraosylceramide, 4 μg; *P1*, pentaosylceramide, 4 μg; Forssman pentaosylceramide, 4 μg; nonacid glycosphingolipids of porcine small intestine (blood group O), 40 μg.

fraction from porcine lung was thereafter separated by Iatrobeads chromatography. Aliquots of the fractions obtained were analyzed by TLC, and fractions that were colored green by anisaldehyde were tested for binding of SadP using the chromatogram binding assay. The fractions were thereafter pooled according to the mobility on thin-layer chromatograms and their SadP-binding activity.

The binding of SadP to neutral glycolipids isolated from porcine lung using TLC overlay assay

The porcine lung nonacid glycosphingolipid fractions were analyzed with type P_N SadP(31-328). The separations gave two SadP-binding fractions migrating in the triglycosylceramide region. One fraction (0.2 mg) migrating as a single band was denoted fraction PL-1 (Fig. 2*B*, *lane 1*), and

Figure 1. Homology of SadP types P_N and P_O galabiose-binding domains and their distribution in systemic, respiratory, and nonclinical *S. suis* isolates. *A,* multiple sequences alignment of SadP galabiose-binding domains of type P_N and type P_O strains. Conserved amino acids are shown in *shaded red rectangles* and *white letters*. Residues with >70% similarity according to their physicochemical properties are framed in *white background with red letters*. Residues involved in hydrogen-bond formation with galabiose (Galα1–4Gal) are shown with a *black triangle* (▲) and those involved in hydrophobic interactions with a *star* (★). Residues 139-343 of SadP are included as found in the crystal structure (PDB code 5BOB). Secondary structure elements are shown on the *top*. The figure was created with ESPript (46). *B,* distribution of SadP-type P_N and P_O alleles in *S. suis* clinical and nonclinical isolates. Maximum-likelihood core genome phylogeny of 374 *S. suis* (12). The phylogeny was run with RAxML using SNP sites. The nucleotide substitution model used was GTR GAMMA. Tips of the tree are colored according to the SadP allele detected with SRST2. *NA* means that with the default parameters neither allele was detected. The *inner circle* shows the phenotype (12). *Gray,* nonclinical; *red*, respiratory; *blue*, systemic (brain); *green*, systemic (other), and *black,* unknown. The *outer circle* is colored according to the SadP allele detected with SRST2 with the same colors as the tree tips. *White*, NA; *red*, P_N, and *black*, P_O.

Table 1
Binding of SadP to glycosphingolipids on thin-layer chromatograms

No.	Trivial name	Structure	SadP type P_N/P_O	Source
1.	Galabiosyl-ceramide Gb2	Galα4GalβCer	–[a]	Human meconium
2.	Gb2-S lipid-linked galabiose	Galα4Galβ–O–*bis*–(SO_2-$C_{16}H_{33}$)$_2$	+/–	Synthetic
3.	Isoglobotriaosyl-ceramide iGb3	Galα3Galβ4GlcβCer	+/–	Cat intestine
4.	Globotriaosyl-ceramide Gb3	Galα4Galβ4GlcβCer	+++/+++	Human RBC[b]
5.	Globotetraosyl-ceramide Gb4	GalNAcβ3Galα4Galβ4GlcβCer	+/–	Human RBC
6.	Forssman	GalNAcα3GalNAcβ3Galα4Galβ4GlcβCer	–	Dog intestine
7.	*para*-Forssman	GalNAcβ3GalNAcβ3Galα4Galβ4GlcβCer	–	Human RBC
8.	P1	Galα4Galβ4GlcNAcβ3Galβ4GlcβCer	+++/+++	Human RBC
9.	H type 4/Globo H hexa	Fucα2Galβ3GalNAcβ3Galα4Galβ4GlcβCer	–	Pig intestine
10.	H type 2 penta	Fucα2Galβ4GlcNAcβ3Galβ4GlcβCer	–	Pig lung
11.	Galili penta	Galα3Galβ4GlcNAcβ3Galβ4GlcβCer	–	Pig lung
12.	Le^b hexa	Fucα2Galβ3(Fucα4)GlcNAcβ3Galβ4GlcβCer	–	Pig lung
13.	Le^y hexa	Fucα2Galβ4(Fucα3)GlcNAcβ3Galβ4GlcβCer	–	Pig lung
14.	A type 2 hexa	Galα3(Fucα2)Galβ4GlcNAcβ3GalβGlcβCer	–	Pig RBC
15.	A type 4 hepta	GalNAcα3(Fucα2)Galβ3GalNAcβ3Galα4Galβ4Glcβ-Cer	–	Pig intestine

[a]Binding is defined as follows: +++ denotes highly reproducible binding of SadP(31-328) type P_N and P_O, when 4 μg of the glycosphingolipid was applied on the thin-layer chromatogram, whereas + denotes an occasional binding, and – denotes no binding even at 4 μg.
[b]Erythrocytes.

one fraction (0.3 mg) migrating as a double band was denoted fraction PL-2 (Fig. 2*B*, *lane 2*). In addition, one SadP-binding fraction (0.4 mg) with compounds migrating as tetraglycosylceramides was obtained (denoted fraction PL-4; Fig. 2*B*, *lane 4*).

LC-ESI/MS of native SadP-binding glycosphingolipids from porcine lung

ESI/MS of the native fraction PL-1 gave a major $[M\text{-}H^+]^-$ ion at *m/z* 1132 (Fig. S1*A*), indicating a glycosphingolipid with three Hex, and sphingosine with nonhydroxy 24:1 fatty acid. MS^2 of the $[M\text{-}H^+]^-$ ion at *m/z* 1132 gave a series of Y ions (Y_0 at *m/z* 646, Y_1 at *m/z* 808, and Y_2 at *m/z* 970) demonstrating a Hex-Hex-Hex sequence combined with sphingosine with nonhydroxy 24:1 fatty acid (Fig. S1*B*).

A $[M\text{-}H^+]^-$ ion at *m/z* 1132 was also obtained by ESI/MS of the native fraction PL-2 (Fig. S2). Here, the major $[M\text{-}H^+]^-$ ion was seen at *m/z* 1022 (Fig. S2, *A* and *B*), demonstrating a glycosphingolipid with three Hex, and sphingosine with nonhydroxy 16:0 fatty acid. Also, here a Hex-Hex-Hex sequence was demonstrated by the series of Y ions (Y_0 at *m/z* 536, Y_1 at *m/z* 698, and Y_2 at *m/z* 860) from MS^2 (Fig. S2*D*).

Endoglycoceramidase digestion and LC-ESI/MS of SadP-binding glycosphingolipids from porcine lung

The base peak chromatograms from LC-ESI/MS of the oligosaccharides obtained by endoglycoceramidase digestion of fractions PL-1 and PL-2 were very similar (Fig. S3, *A* and *B*). Both had a $[M\text{-}H^+]^-$ ion at *m/z* 503, which eluted at the same retention time (17.4-18.4 min) as the saccharide obtained from reference globotriaosylceramide (Fig. S3*C*), whereas the saccharide from reference isoglobotriaosylceramide eluted at 20.0-20.4 min (Fig. S3*D*).

MS^2 of the ion at *m/z* 503 of fractions PL-1 and PL-2 gave in both cases two C-type fragment ions (C_1 at *m/z* 179 and C_2 at *m/z* 341) identifying a Hex-Hex-Hex sequence (Fig. S3, *E* and *F*). A 4-substitution of the internal Hex was demonstrated by the $^{0,2}A_2$ fragment ion at *m/z* 281 (20–22). Taken together with the similarity to the MS^2 spectrum of reference globotriaosyl saccharide (Fig. S3*G*), this allowed identification of the saccharides of fractions PL-1 and PL-2 as globotriaosyl saccharides (Galα1–4Galβ1–4Glc).

LC-ESI/MS of the oligosaccharides obtained by hydrolysis of fraction PL-4 with *Rhodococcus* endoglycoceramidase II allowed a tentative identification of a globotetra saccharide (GalNAcβ1–3Galα1–4Galβ1–4Glc). This conclusion was based on the following spectral features. First, the base peak chromatogram of fraction PL-4 had a $[M\text{-}H^+]^-$ ion at *m/z* 706 (Fig. S4*A*), and MS2 of this ion (Fig. S4*B*) gave a C-type fragment ion series (C_1 at *m/z* 220, C_2 at *m/z* 382, and C_3 at *m/z* 544), demonstrating a HexNAc-Hex-Hex-Hex sequence. The $^{0,2}A_3$ fragment ion at *m/z* 484 demonstrated a 4-substituted Hex, whereas the $^{0,2}A_4$ ion at *m/z* 646, and the $^{0,2}A_4$-H_2O ion at *m/z* 628 were derived from cross-ring cleavage of the 4-substituted Glc of the lactose unit at the reducing end. The features of this MS^2 spectrum were very similar to the MS^2 spectrum of the reference globotetra saccharide (Fig. S4*C*).

The base peak chromatogram of fraction PL-4 (Fig. S4*A*) also had two $[M\text{-}H^+]^-$ ions at *m/z* 998, eluting at 19.4 and 21.4 min. In both cases MS^2 demonstrated a Fuc.Hex-(Fuc-)HexNAc-Hex-Hex sequence, and the diagnostic ion at *m/z* 348 (Fig. S4*D*) identified a Le^b hexasaccharide, whereas the diagnostic ion at *m/z* 510 (Fig. S4*E*) identified a Le^y hexasaccharide (21).

SadP subtype P_N and P_O binding to purified glycolipids

TLC overlay assay is a powerful method to analyze glycolipid receptor function. The carbohydrate-binding specificity of SadP to globo series isoreceptors was determined using purified glycolipids (all TLC binding results are summarized in Table 1). Type P_N SadP(31-328) bound preferentially to Gb3 and P1 glycolipid, and also weakly to Gb4 and the Forssman glycolipid (Fig. 2*C*). Type P_O SadP(31-328) also bound strongly to Gb3 and P1, *i.e.* to glycolipids with terminal Galα1–4Gal, whereas there was no binding to Gb4 and the Forssman glycolipid (Fig. 2*D*). There was no binding to the nonacid glycolipid fraction from the pig intestine, containing the globo H.

The type P_N 76-kDa full-length SadP and SadP(31-328) binding to dilutions of globo series glycolipids was analyzed with TLC overlay assay to the detection limit for the various glycolipids (Fig. S5*A*). The full-length adhesin bound mainly to P1 glycolipid,

with a detection limit at 0.4 μg, whereas the detection limit for the Gb3 glycolipid was 0.8 μg. The detection limit of SadP(31-328) N-terminal domain was 0.2 μg for both Gb3 and P1.

Next, the type P_N SadP(31-328) binding to 250 ng of glycolipids immobilized in plastic microtiter wells was quantitatively evaluated by a solid phase-binding assay (Fig. S5*B*). No binding to the Gb2 glycolipid, galabiosylceramide, was detected, whereas there was weak binding to Galα1–4Galβ1–*O-bis*-$(SO_2\text{-}C_{16}H_{33})_2$. SadP was found to bind stronger to Gb3 with nonhydroxy ceramide than to Gb3 with hydroxy ceramide. There was also binding to Gb4 and iGb3 isoglobotriaosylceramide. Binding to P1 pentaosylceramide was at the same level as binding to Gb3 with nonhydroxy ceramide. The difference in the binding to iGb3 (Galα1–3Gal- containing glycolipid) in the microtiter well assay compared with TLC overlay assay could be due to the difference in the presentation of the binding epitope and the clustering of the glycolipid moieties.

Galα1–4Gal–dependent endothelial cell-binding activity of S. suis SadP-type P_N

S. suis-type P_N WT strain D282 and the corresponding mutant strain D282Δ*sadP,* containing an insertion mutation into SadP gene, were compared for their binding activity to cultured cell line EA.hy926, which is a primary human umbilical vein cell line fused with a thioguanine-resistant clone of A549 (human lung adenocarcinoma cell line). In addition, binding of purified fluorescently labeled SadP was analyzed for the binding to EA.hy926 cells. The cells were grown into glass coverslips for 48 h and the bacteria grown into early log phase were added to cells and left to adhere for 1 h. After washing and staining with DiffQuick, the bacteria were enumerated. The average adherence of WT bacteria was calculated to be 8.7 ± 0.5 bacteria/field, whereas the mean adhesion of 1.3 ± 0.5 of the insertion mutant Δ*sadP* was significantly less (unpaired *t* test >0.0001) (Fig. 3*A*). In addition, the binding of the WT strain was inhibited with 10 μg/ml of pigeon ovomucoid, which contains *N*-linked glycans with terminal Galα1–4Gal (23). The inhibitor reduced the adherence of *S. suis* bacteria to the cells to 0.7 ± 0.1 bacteria/field.

For flow cytometry assay, the cells were grown in wells, washed, and tested for the binding of FITC-labeled type P_N SadP(31-328). After washing, the cells were harvested with scraping and analyzed with flow cytometer. The flow cytometry results (dot blot and the histogram) are presented in Fig. 3. *B–D*. The median SadP binding with and without inhibitor (pigeon ovomucoid, 10 μg/ml) were 56.2 and 14.9 per 10,000 total events (median of untreated cells was 12.8).

Fine specificities toward Gb3 and Gb4 oligosaccharide structures

Next, the ability of the type P_N SadP-D282(31-328) and P_O SadP-6407(31-328) recombinant adhesin constructs to recognize galabiose glycoconjugates was analyzed using isothermal titration calorimetry (Fig. 4, *A* and *B*). Both type P_N and P_O adhesins were titrated with oligosaccharides representing the terminal epitopes of Gb3 and Gb4, the TMSEt (2-trimethylsilylethyl)glycosides) of Galα1–4Gal and GalNAcβ1–3Galα1–4Gal (24). The dissociation constant values (K_D) of type P_N SadP-D282(31-328) and type P_O SadP-6407(31-328) interaction with Galα1–4Gal were 13.0 ± 1.5 μM (n = 0.85, ΔH = −69.0 ± 2.0 kcal/mol and $-T\Delta S$ = 41.1 kcal/mol) and 3.5 ± 1.6 μM (n = 0.85, ΔH = −40.0 ± 2.7 kcal/mol and $-T\Delta S$ = 8.8 kcal/mol), respectively. The K_D for interaction of P_N and P_O adhesins with GalNAcβ1–3Galα1–4Gal compared with Galα1–4Gal were 2.6-fold higher with type P_N (K_D = 33.7 ± 3.5 μM, n = 1.14, ΔH = −40.1 ± 2.0 kcal/mol and $-T\Delta S$ = 14.0 kcal/mol) and 269 higher with type P_O (K_D = 940 ± 680 μM, n = 0.13, ΔH = −197 ± 5500 kcal/mol and $-T\Delta S$ = 179 kcal/mol).

Then, both adhesins were analyzed with AlphaScreen competitive inhibition assay (Fig. 4*C*) for their interaction with Galα1–4Gal compared with a glycomimetic inhibitor 3′-phenylurea-derivative (3'-phenylurea-Galα1–4Galβ1–methoxyphenyl), which is a low nanomolar inhibitor of type P_N SadP (19, 25). The binding of His-tagged recombinant adhesins to biotinylated pigeon ovomucoid was inhibited with the above oligosaccharides. The IC_{50} values of type P_N adhesin for Galα1–4Galβ1–methoxyphenyl and 3'-phenylurea-Galα1–4Galβ1–methoxyphenyl were 1 and 0.030 μM, whereas with type P_O adhesin the corresponding values were 0.3 and 70 μM, respectively. Also 4 other recombinant type P_O SadP N-terminal domains were tested using 10 μM inhibitor concentrations (Fig. 4*D*). For all type P_O adhesins the inhibition obtained with the C3'-phenylurea-derivative was weaker than the inhibition obtained with Galα1–4Gal.

Site-specific mutation changes the specificity of type P_N recombinant adhesin to type P_O

The binding mechanism of type P_N and P_O SadP was further studied by site-directed mutagenesis. Type P_N adhesin SadP-D282(125-329) was mutated and the mutants were analyzed for the binding to galabiose oligosaccharides with AlphaScreen competitive inhibition assay and ITC. Multiple alignment of SadP homologues allowed us to predict amino acids from the galabiose-binding region that differed between types P_N and P_O (Fig. 1*A*). Based on that, the site-specific amino acid changes for N285D and E292Q, deletion Δ244-246 & N285D, and Δ244-246 mutants were constructed into the type P_N SadP (125-328) cloned into the plasmid pET28a. In addition, the 28-amino acid long region His-216–Asp-246 of the type P_N was replaced by the corresponding region of type P_O.

The WT SadP and mutants were expressed and purified as described under "Experimental procedures" and analyzed with SDS-PAGE (Fig. S6). The galabiose-binding strengths of the above mutant constructs, full-length SadP, SadP N-terminal constructs SadP(31-328), SadP(125-328), and as a negative control site-specific mutant SadP(31-328)W258A, were compared by AlphaScreen asssay (Fig. S7*A*). The binding of full-length SadP to biotinylated pigeon ovomucoid was weaker compared with the N-terminal domain constructs, which could be due to a larger size of the full-length SadP. The size of the protein could increase the distance of the acceptor and donor beads, and hence reduce the transmission of the singlet oxygen during the assay (19). As a negative control for the assay, there was no binding of site-specific mutant W258A to pigeon ovomucoid. Of the mutants in the type P_N SadP(125-328) background, mutants N285D and E292Q bound well, whereas the binding of

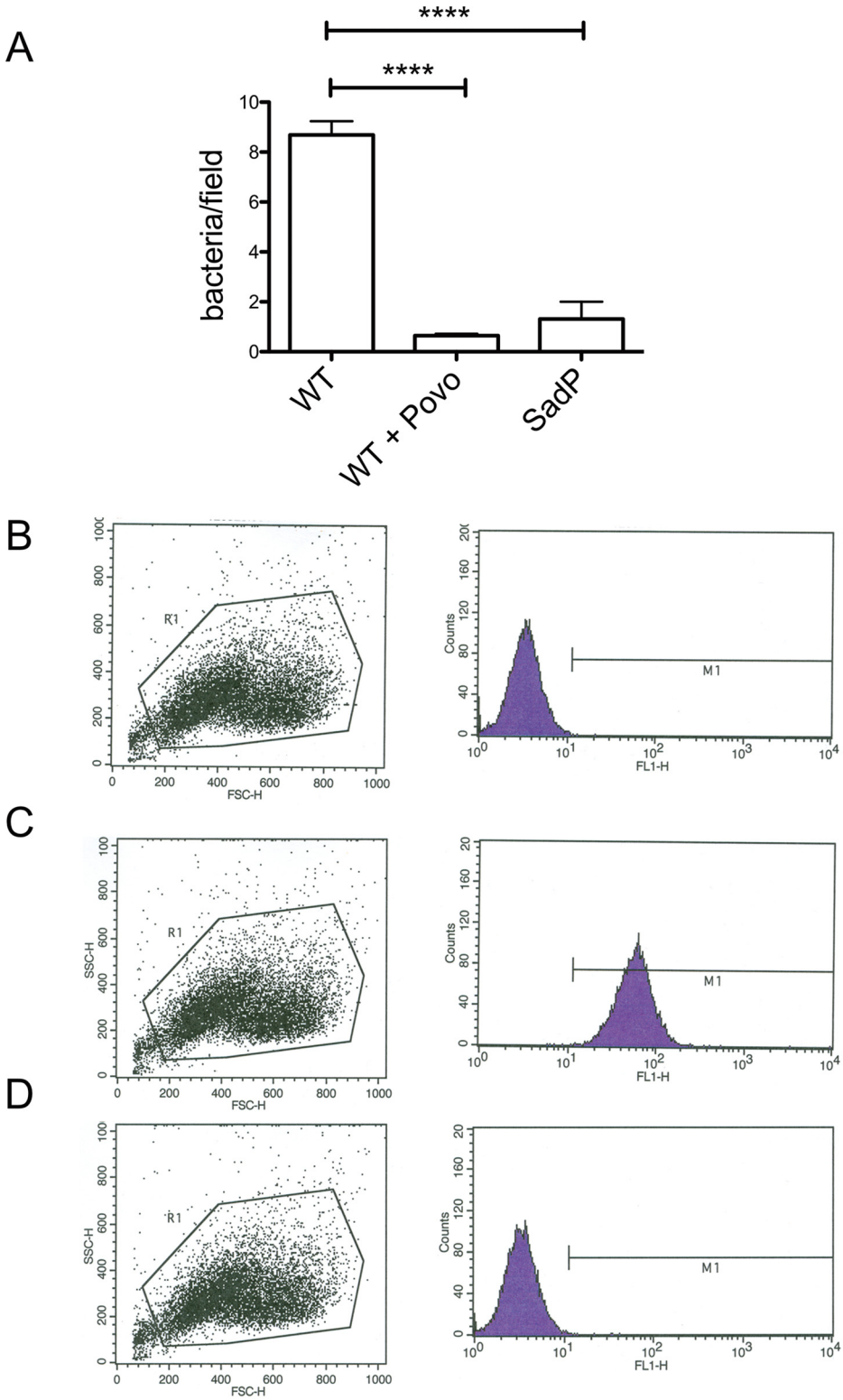

Figure 3. SadP binding to the EA.hy926 cell line. *A,* binding of *S. suis* D282 WT serotype 2 strain and the SadP insertion mutation to EA.hy926 cells grown on coverslips. The binding of the WT bacteria was inhibited with 10 μg/ml of pigeon ovomucoid. Flow cytometry analysis of SadP(31-328)-type P_N binding to EA.hy926 cells. *B,* buffer control. *C,* SadP adhesin (0.4 μg/ml) and *D,* SadP adhesin in the presence of 10 μg/ml of pigeon ovomucoid.

mutants Δ244-246 and H216-D246delinsDELFNRFPNKVD-STNNGDGAPFRFFNKE was reduced. The binding of the N285D/Δ244-246 mutant was abolished.

Next the specificities of mutants were analyzed with AlphaScreen assay using the phenylurea derivative and Galα1–4Gal (Fig. S7, *B–F*). All mutants were equally inhibited by

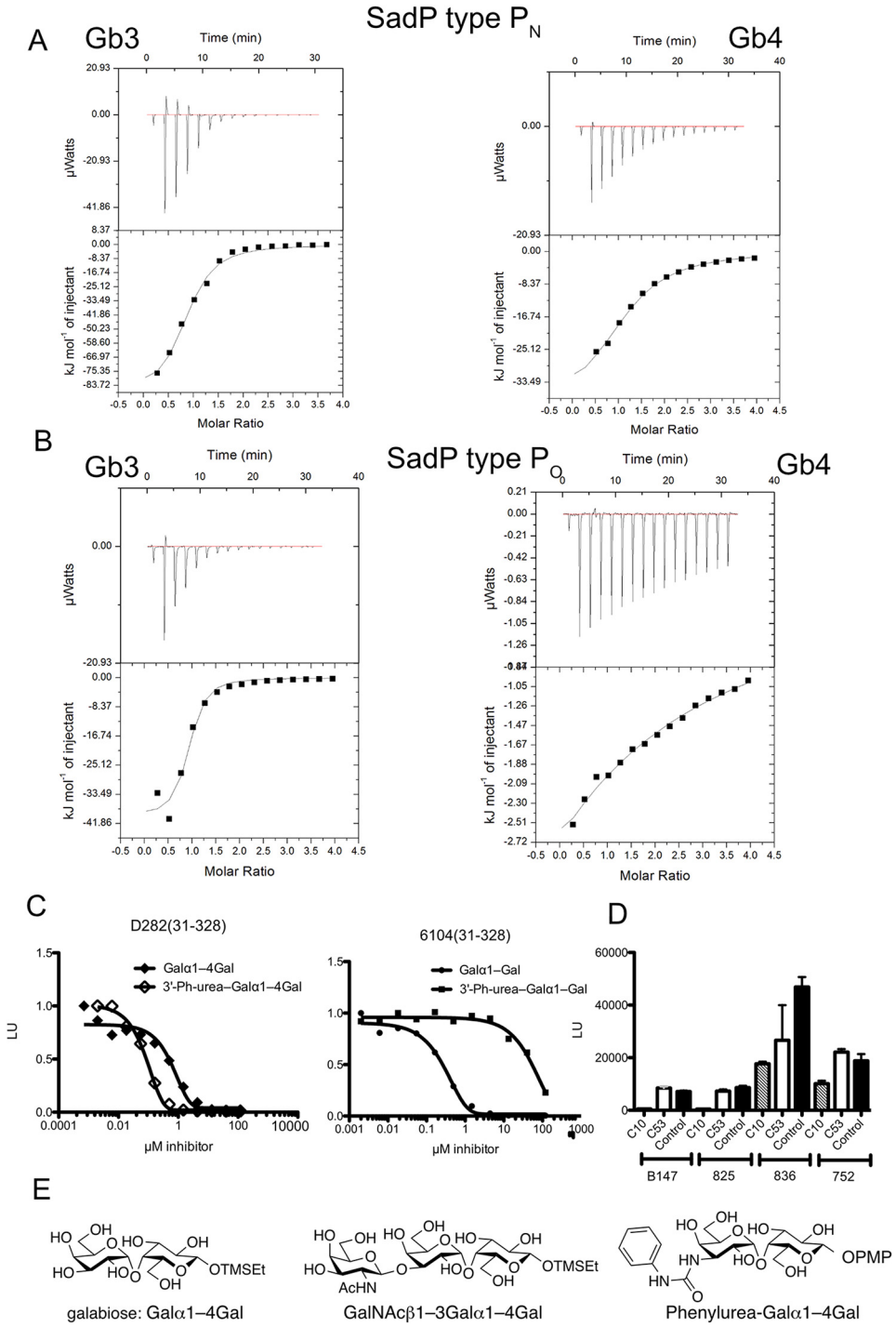

Figure 4. Oligosaccharide specificity of SadP from systemic (type P_N) and respiratory (type P_O) *S. suis* strains analyzed with glycans representing the terminal saccharide structure of Gb3 and Gb4. *A* and *B*, ITC of SadP-type P_N and type P_O with Galα1–4Galβ1– and GalNAcβ1–3Galα1–4Galβ1–TMSEt derivatives. *C*, AlphaScreen inhibition assay with Galα1–4Galβ1– and 3'-phenylurea-Galα1–4Galβ1–methoxyphenyl (-PMP = 4-methoxyphenyl). *D*, AlphaScreen inhibition assay of Galα1–4Galβ1– (compound C10) and 3'-phenylurea-Galα1–4Galβ1–methoxyphenyl (compound C53) with recombinant N-terminal domains cloned from 4 different type P_O *S. suis* strains. *E*, structures of the ligands in this study.

the Galα1–4Gal oligosaccharide, but only with the site-specific mutant N285D the inhibitory power of phenylurea-Galα1–4Gal was weaker compared with Galα1–4Gal, suggesting a specific switch from type P_N to P_O specificity.

Next, the AlphaScreen inhibition assay was used to compare the effect of site-specific mutation in N285D to the specificity between Galα1–4Gal (terminal Gb3 structure) and GalNAcβ1–3Galα1–4Gal (terminal Gb4 structure) TMSEt glycosides. SadP(125-329) type P_N and the site-specific mutant N285D were similarly inhibited with Galα1–4Gal, whereas N285D was not inhibited with even higher concentrations of GalNAcβ1–3Galα1–4Gal (Fig. 5, *A* and *B*).

The K_D values of type P_N SadP(125-328) and site-specific mutant N285D for oligosaccharides was analyzed with

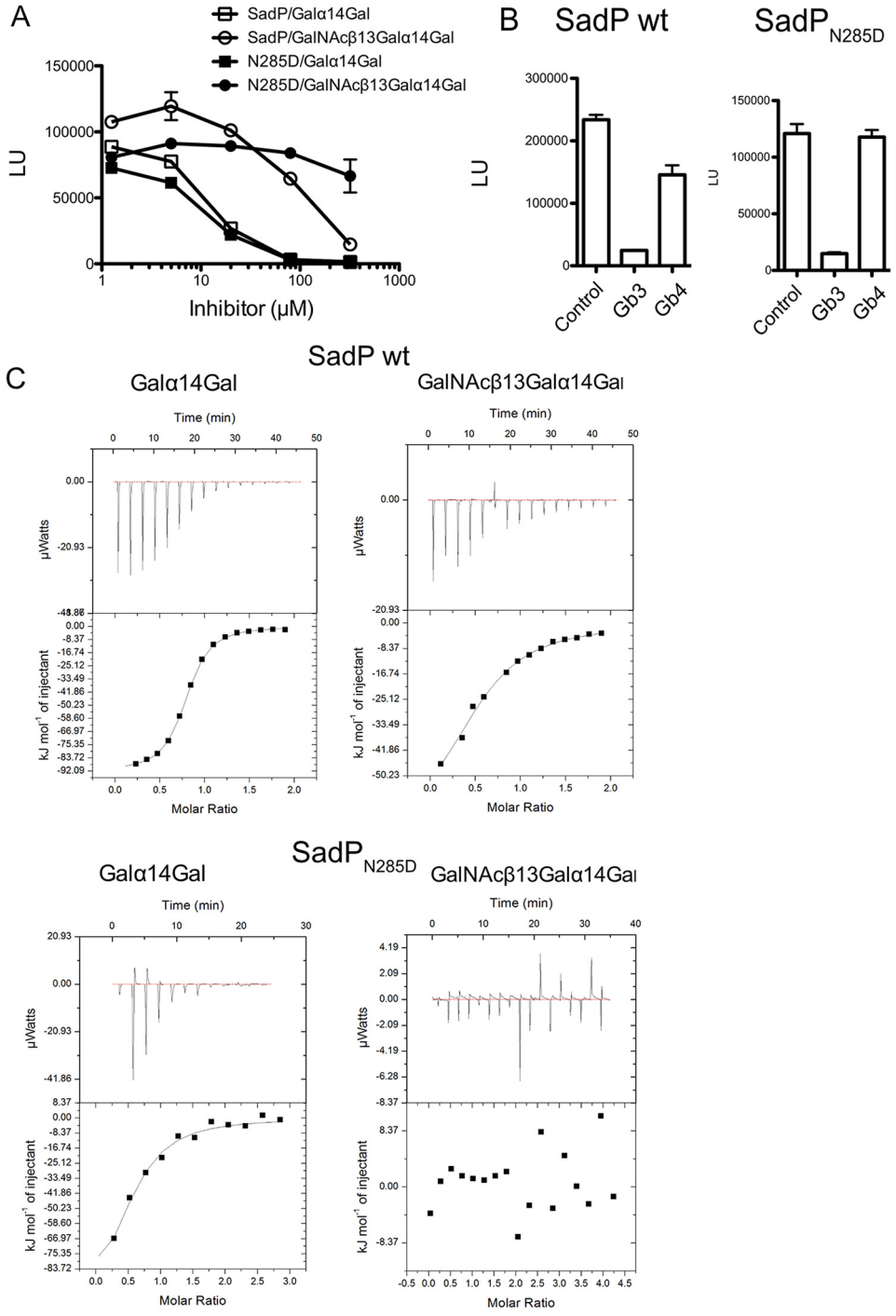

Figure 5. A single amino acid site-specific mutation N285D of SadP from systemic strains changes its Gb4 binding specificity to type P_O Gb3 binding specificity of respiratory strains. *A,* inhibition of WT SadP(125-329) and its site-specific mutant SadP(125-329)N285D with the dilutions series (1.25 to 320 μM, duplicate determinations) of TMSEt glycosides of Galα1–4Gal and GalNAcβ1–3Galα1–4Gal representing the Gb3 and Gb4 oligosaccharides. *B,* inhibition assay with 5 μM Galα1–4Gal and GalNAcβ1–3Galα1–4Gal TMSEt glycosides. *C,* ITC measurements of WT SadP and N285D mutant with the TMSEt glycosides of Galα1–4Gal and GalNAcβ1–3Galα1–4Gal representing the Gb3 and Gb4 oligosaccharides.

isothermal titration calorimetry (Fig. 5*C*). The WT SadP(125-329) K_D values for Galα1–4Gal and GalNAcβ1–3Galα1–4Gal were 3.4 ± 0.09 (n = 0.76, ΔH = 92.0 ± 0.3 kcal/mol and $-T\Delta S$ = 60.8 kcal/mol) and 36.0 ± 4.8 μM (n = 0.56, ΔH = 70.2 ± 5.0 kcal/mol and $-T\Delta S$ = 44.7 kcal/mol), respectively. The K_D of site specific mutant N285D with Galα1–4Gal was 22.7 ± 7.2 μM (n = 0.52, ΔH = 26.8 ± 5.4 kcal/mol, and $-T\Delta S$ = 20.5 kcal/mol) (6-fold increase compared with WT SadP), whereas there was no interaction between N285D and GalNAcβ1–3Galα1–4Gal. Thus, the above results suggest that Asn-285 has a specific role in SadP-type P_N binding to GalNAcβ1–3Galα1–4Gal.

The effect of N285D mutation to SadP binding to glycolipids incorporated into POPC and POPC-cholesterol liposomes

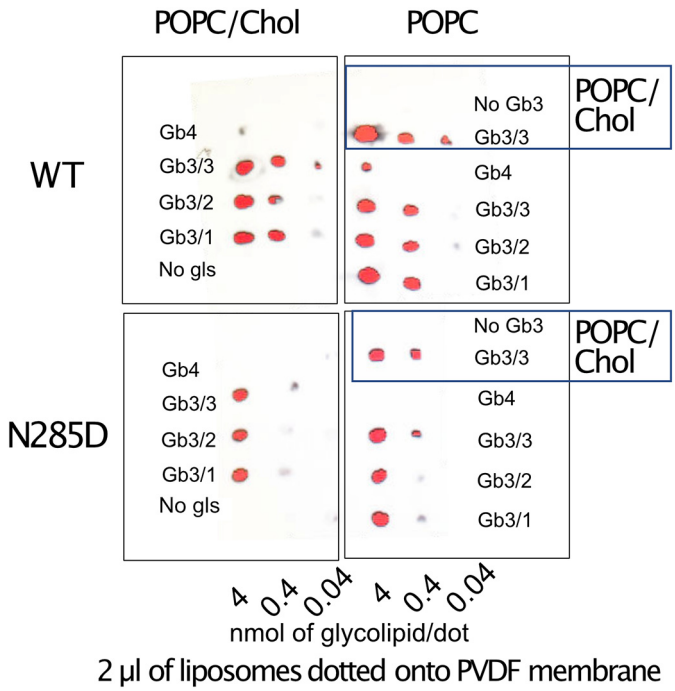

Figure 6. SadP and SadP/N285D binding to liposomes. POPC/glycolipid liposomes (4, 0.4, and 0.04 nmol/dot) and POPC/cholesterol/globosylceramide liposomes (4, 0.4, and 0.04 nmol/dot) were applied onto PVDF membrane. *WT*, His-tagged SadP(125-329) type P_N; *N285D*, site-specific mutant of SadP(125-329); replicate membranes containing dotted liposomes with or without cholesterol (see "Experimental procedures") were probed with SadP and SadP/N285D. The bound proteins were detected with anti-His and horseradish peroxidase-labeled antibodies as described under "Experimental procedures" and the membrane was imaged with FujiLAS-4000. The globo series glycolipids used were: *Gb4*, d18:1-24:0 + d18:1–16:0; *Gb3/1*, Gb3 d18:1-24:0; *Gb3/2*, Gb3 d18:1-16:0; *Gb3/3*, Gb3 d18:1-h16:0.

was analyzed by dotting liposomes to PVDF membrane and binding of His-tagged adhesins to immobilized liposomes (Fig. 6). WT SadP-type P_N bound to Gb4 of both noncholesterol and cholesterol-containing liposomes, whereas there was no binding by N285D mutant. The acyl chain length or hydroxylation of ceramide had no major effects for Gb3 binding.

Structural comparison of recombinant SadP-type P_N and its N285D mutant

The site-specific mutant SadP(125-329)/N285D was crystallized with five molecules in the crystallographic asymmetric unit (Fig. 7*A*, Table S1). All molecules are similar with subtle differences as suggested by the low root mean square deviation (RMSD) between them (0.25-0.31 Å). The structure of the N285D mutant is similar to that of the native SadP (PDB code 5BOB) with RMSD of 0.26 Å for 199 aligned residues. The structure consists of three α-helices and 10 β-strands ($\beta1$-$\beta10$) that form a β-sandwich core domain (Fig. 7*B*). The first β-sheet of the β-sandwich is formed by antiparallel $\beta1$-$\beta10$-$\beta9$-$\beta4$-$\beta7$-$\beta6$ strands and the second β-sheet by $\beta2$-$\beta3$-$\beta8$-$\beta5$ in antiparallel fashion.

Structural superposition with the Galα1–4Gal–Fhc structure revealed small differences (Fig. 7*C*). The side chain of Asp-285 was found slightly rotated compared with the Asn-285 side chain in the WT.

Resolution of the interaction mechanisms of SadP to globo series glycolipids and C3′-phenylurea–Galα1–4Gal

The key amino acids of both types P_N and P_O are conserved. Tyr-198, Gln-255, Arg-238, and Gly-233 forms hydrogen bonds with the HO–3′, HO–4′, and HO–6′ of the α'-Gal and the Lys-316 with HO–2 and HO–3 of the β-Gal pyranose ring. Trp-258 most likely forms CH-π interactions with the hydrophobic face of the disaccharide (Fig. 7*C*). Type P_N SadP Asn-285 is on the edge of the binding pocket, and it potentially interacts with the terminal GalNAcβ1–3 of Gb4 or 3-phenylurea group. To study the SadP interaction with the receptor saccharide Galα1–4Galβ1–4Glc in solution, STD-NMR was applied using type P_N SadP(125-329) and the corresponding mutant N285D (Fig. 7*D*). STD-NMR results suggest that both the type P_N SadP and the mutant N285D interact mainly with the two terminal galactose units of Gb3. With the mutant N285D the interactions of H–4′ and H–4″ are, however, somewhat weaker compared with the interaction of H–6″. Additionally, the mutant N285D does not seem to have a clear interaction with the β-glucoside unit at the reducing end of Gb3, whereas the type P_N SadP appears to have interactions with H–2, H–3, and H–4.

To find a plausible hypothesis explaining the binding preferences of the galabiose, GalNAcβ1–3Galα1–4Gal, and phenylurea-galabioside for WT and the N285D mutant, molecular dynamic simulations of their respective complexes were performed. Briefly, the ligand structures were built without the TMSEt or methoxyphenyl aglycons to simplify the simulations and were then placed in the binding site of SadP (PDB code 5BOA) with the Galα1–4Gal disaccharide oriented as in the crystal structure. The terminal GalNAcβ1 residue was oriented with the dihedral glycosidic bond angles minimized with the H1 parallel to H4′ of Galα1–4Gal. The three complexes with WT were mutated by exchanging Asn-285 for Asp-285. The complexes were unrestrainedly subjected to 100-ns molecular dynamics simulations and all starting conformations converged toward similar stable complex geometries (Fig. 8, *A-E*), except for the phenylurea derivative in complex with the N285D mutant for which light constraints on the backbone atoms of protein secondary structures were applied (Fig. 8*F*). The α-face of the β-galactoside residue of all three ligands stacked to Trp-258 forming CH-π interactions and the galabiose disaccharide moiety in all simulations retained the interactions and hydrogen bonds observed in the X-ray structure with the Gb3 trisaccharide (PDB ID 5BOA). The HO–4′ of galabiose did not interact directly with Asn-285, but instead via Asn-285 side chain NH hydrogen bond donation to a network of hydrogen bonds involving 3-5 water molecules and the Gly-233 carbonyl oxygen (Fig. 8*A* and Movie S1). Mutation of Asn-285 to Asp-285 influenced the directionalities of the hydrogen bonding partners in this network (Fig. 8*D* and Movies S2), which may explain the different STD-NMR data with WT and the Asp-285 mutant. The simulations with the GalNAcβ1–3Galα1–4Gal and the phenylurea-galabioside in complex with the WT protein converged to geometries that revealed a highly populated interaction between the ligands and Asn-285. The ring oxygen of the GalNAc residue of the trisaccharide and the urea carbonyl oxygen of the phenylurea derivative accepted hydrogen bonds

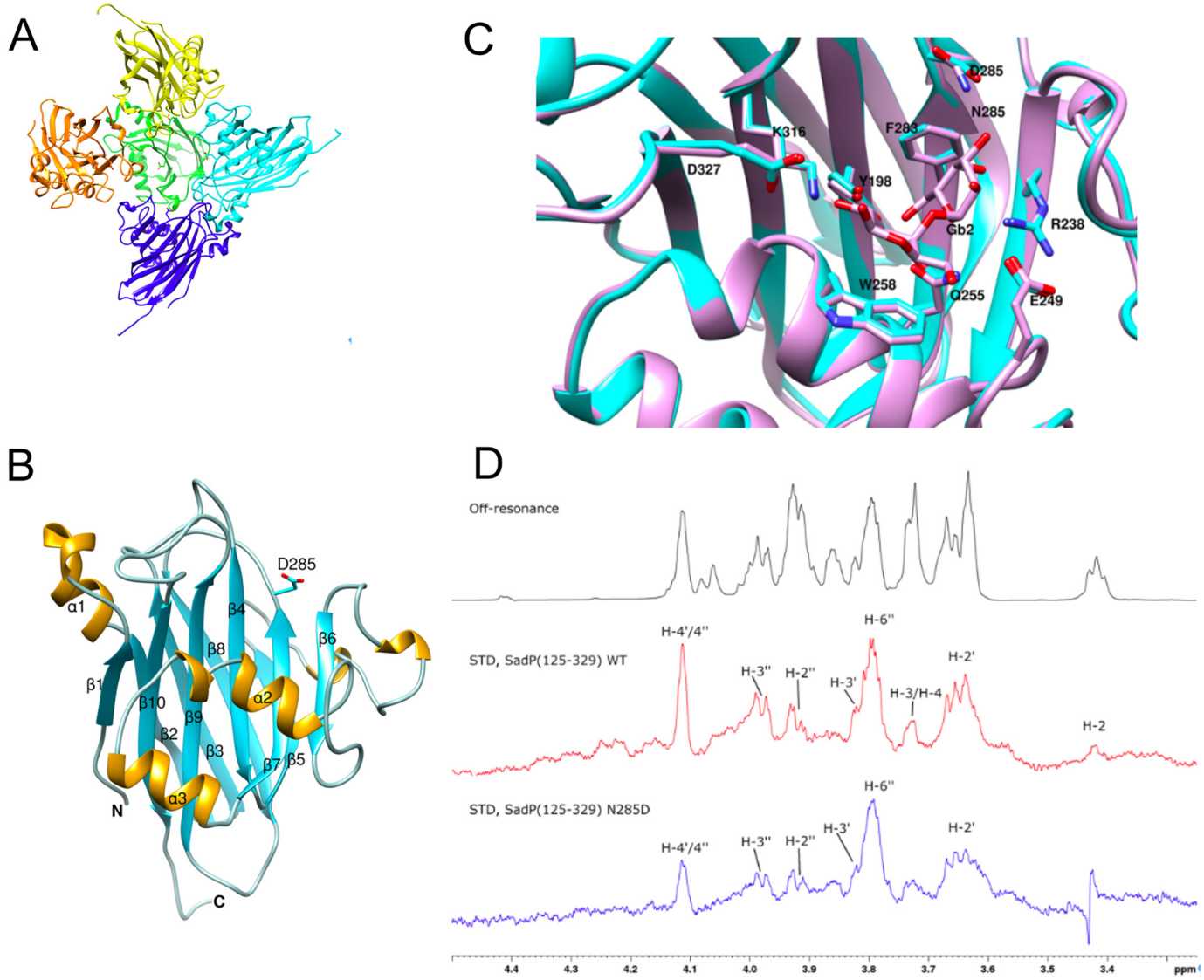

Figure 7. *A*, arrangement of the five site-specifically mutated SadP(125-329)/N285D molecules in the crystallographic asymmetric unit. Each molecule is shown as *ribbon* and colored differently. *B*, ribbon diagram of SadP(125-329)/N285D structure. α-Helices are shown in *yellow color* and β-strands in *cyan*. Asp-285 is depicted as *sticks*. *C*, structural superposition of Galα1–4Gal-bound Fhc (PDB 5BOA) structure (identical to SadP-type P_N (*pink*) onto SadP(125-329)/N285D (*cyan*). Residues involved in binding interactions are shown in stick representation. *D*, STD-NMR of binding of WT SadP(125-329) type P_N and its site-specific mutant N285D. Peaks in the STD spectra indicate hydrogens (C-H) that are in close proximity to the protein.

from the Asn-285 side chain NH_2 (Fig. 8, *B* and *C*, and Movies S3 and S4). The GalNAc HO-4 of the trisaccharide formed transient hydrogen bonds to side chain amide groups of Glu-286 and Glu-234, whereas the phenyl ring of the phenylurea ligand did not form any persistent interactions with any protein residue. The highly populated hydrogen bonds of the trisaccharide GalNAc ring oxygen and the phenylurea carbonyl oxygen to Asn-285 could not form in the N285D mutant (Fig. 8, *E* and *F*, and Movies S5 and S6). Instead, it was disrupted by the formation of a water network between the Asp-285 side chain carboxylate and the GalNAc ring oxygen of the trisaccharide (Fig. 8*E*), whereas the phenylurea moiety of the phenylurea galabioside rotated away from the Asp-285 side chain carboxylate (Fig. 8*F*). This lack of direct hydrogen bond interactions of the GalNAc ring oxygen and urea carbonyl oxygen may at least partly explain the less efficient binding of the trisaccharide and phenyl urea derivative to the N285D mutant.

Discussion

SadP carbohydrate specificity to neutral glycolipids from lungs was studied by TLC overlay assay. The carbohydrate receptors for *S. suis* adhesion in the respiratory tract and lungs have remained elusive. We studied here how SadP-type P_N and P_O recognize glycolipids isolated from pig lung. The major pig lung neutral glycolipids were identified as Gb3, Gb4, the H type 2 pentaosylceramide, the Galili pentaosylceramide, and Le^b and Le^y hexaosylceramides (Fig. 2). In TLC overlay assay, type P_N SadP bound to Gb3 and Gb4, whereas type P_O SadP bound only to Gb3. Both SadP types showed no binding to Galα1–3Gal-containing Galili pentaosylceramide (Fig. 2, *A* and *B*, Table 1).

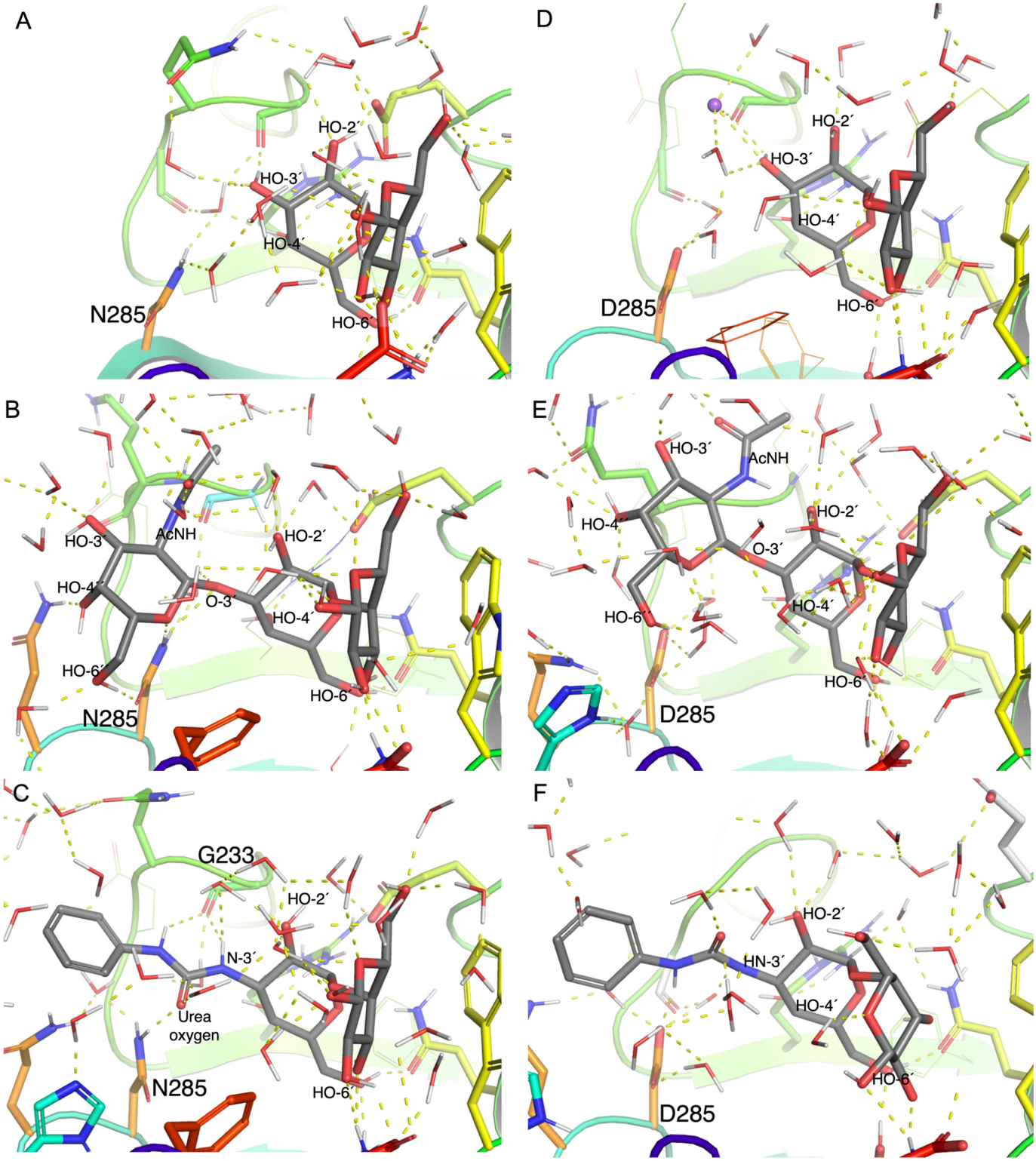

Figure 8. Molecular dynamics of SadP-type P_N binding to Gb4 saccharide and glycomimetic phenylurea-galabiose inhibitor. Representative MD snapshots (at 90 ns) of SadP are shown. WT in complex with: *A*, Galα1–4Gal; *B*, GalNAcβ1–3Galα1–4Galβ; *C*, C3′-phenylurea-Galα1–4Galβ. Representative MD snapshots of SadP/N285D in complex with: *D*, Galα1–4Gal; *E*, GalNAcβ1–3Galα1–4Galβ; and *F*, C3′-phenylurea-Galα1–4Galβ.

Therefore, our findings suggest that globo series glycolipids are the major carbohydrate receptors for *S. suis* in pig lung. Although fucose-binding lectins have been described both in bacterial and fungal lung pathogens, no fucose-specific binding activity was found in SadP. The globo series glycolipids have been shown to be widely expressed in many tissues of pigs (26); hence, they can potentially serve as SadP receptors for other host organs and brain capillary veins critical for *S. suis* invasive infection. We

show that the binding of type P_N *S. suis* serotype 2 *sadP*-mutant to the endothelial cell line was significantly reduced and binding of both the WT *S. suis* bacteria and recombinant SadP adhesin were inhibited with the galabiose-containing pigeon ovomucoid.

The oligosaccharide inhibition assays performed with both whole bacteria and recombinant adhesin suggest that the reducing end β-Glc of Gb3 is required for optimal binding (16, 19). The TLC overlay assay using purified glycolipids showed that SadP bound strongest to the P1 glycolipid (Fig. 2, *B* and *C*, and Fig. S5*A*). The preferential binding to the P1 glycolipid might also be due to a more optimal presentation of the epitope on the longer core chain, whereas hindered presentation of the binding epitope in galabiosyl ceramide might explain why SadP did not bind to Gb2 in the TLC overlay assay. The presence of the P1 structure is not well known in pig, however, it was found in α1,3GalT knockout pig kidney, because this glycosyltransferase is a direct competitor of α1,4GalT (27). This might be important for surveillance of pathogens in xenotransplantation.

The fine specificity of SadP subtypes was further analyzed with ITC and competitive inhibition assay. The ratio of K_D values (Galα1–4Gal/GalNAcβ1–3Galα1–4Gal) for type P_N SadP was 0.4, whereas for type P_O it was 0.004, which is in accordance to the corresponding hemagglutination inhibition MIC values observed with bacterial hemagglutination assays (16). Moreover, the IC_{50} values for Galα1–4Gal and 3'-phenylurea-Galα1–4Gal are in accordance to previous hemagglutination inhibition MIC concentrations for type P_N and P_O *S. suis* (25).

The mechanism of how the two SadP subtypes differ in their recognition of Gb3, Gb4, and glycomimetic 3-phenylurea-galabiose has not been studied before. The multiple sequence alignment of SadP showed that specific amino acids: Gly-233, Glu-249, and Asn-285 of type P_N in the galabiose-binding domain are different compared with type P_O SadP (Fig. 1*A*). Of these, only substitution from asparagine to aspartate at position 285 was found in all hemagglutinating type P_O adhesins. To analyze the mechanisms how SadP-type P_N can bind to Gb4 terminal trisaccharide (GalNAcβ1–3Galα1–4Gal) and 3'-phenylurea-galabiose, we designed mutations to type P_N SadP and analyzed their binding to galabiose. The SadP-type P_N region from His-216 to Asp-246 was swapped to the corresponding region of type P_O (to contain substitution from amino acid Gly to Asn at position 233). The binding of this mutant to galabiose was reduced compared with the WT adhesin (Fig. S7*A*), but was still sufficient to further analyze the oligosaccharide specificity. Deletion Δ244-246 and site-specific mutations N285D and E292Q bound also to galabiose at a sufficient level (Fig. S7*A*) allowing testing with 3'-phenylurea-derivative to compare for type specificity. Of these mutants, only N285D lost the ability to be efficiently inhibited by 3'-phenylurea-derivative (Fig. S7, *B–F*), suggesting that Asn-285 has an important role in interacting with the phenylurea group. The amino acid region 216-246 including G233N substitution have possibly no significant role alone in the interaction with HO–3'-substituted phenylurea-galabiose. However, Gly-233 could still synergistically interact with phenylurea. Therefore, the N285D mutant was chosen for further studies for the type P_N binding mechanism. The WT and N285D mutant were compared for their binding to the soluble Gb4 terminal trisaccharide GalNAcβ1–3Galα1–4Gal and to globo series glycolipids Gb3 and Gb4 (Figs. 5 and 6). The results show consistently that Asn-285 plays a specific role in Gb4 binding as demonstrated by competitive inhibition assay, ITC and liposome binding assay.

Molecular dynamics calculations were performed with the structures representing type P_N SadP(125-329) and its N285D site-specific mutant. Both proteins were analyzed with Galα1–4Gal, GalNAcβ1–3Galα1–4Gal, and 3'-phenylurea-Galα1–4Gal. In accordance to the co-crystal structure (PDB ID 5BOA), the galabiose HO–4', HO6', HO–2, and HO–3 were hydrogen bonded to Tyr-198, Gly-233, Arg-238, Gln-255, and Lys-316. Hydrophobic interaction with the α-face of the β-galactoside stacked to Trp-258 forming CH-π interactions. The above interactions were conserved in WT and Asn-285 mutant. WT SadP Asn-285 formed hydrogen bonds to the GalNAc O–5 ring oxygen of GalNAcβ1–3Galα1–4Gal and to urea's carbonyl group (Fig. 8*B*). The amino acid Asp-285 of a site-specific mutant formed hydrogen bonds with solvent water molecules when simulated with GalNAcβ1–3Galα1–4Gal and 3'-phenylurea-Galα1–4Gal. These results together with the AlphaScreen and ITC data give us a plausible explanation for the molecular mechanism of how type P_N SadP interact with Gb4 terminal GalNAc and with the phenylurea-galabiose derivative. In addition, WT SadP amino acid Gly-233 interacts with the terminal GalNAc of Gb4 via hydrogen bond to the N-acetyl group or to urea's -NH group (Fig. 8*C*).

SadP does not have any sequence homologs in other galabiose-recognizing proteins, however, structurally *E. coli* PapG and SadP galabiose-binding sites share some similarities. They both contain a β-sheet composed of antiparallel β-strands, which are adjacent to the galabiose-binding domain (PDB; *E. coli* 1J8R, *S. suis* 5BOA). In SadP, the binding site is formed by the α-helix and a nonhelix loop, whereas in PapG the galabiose-binding site is located in the middle of two nonhelix loops. Other galabiose-binding proteins such as *P. aeruginosa* LecA (4YW6), *E. coli* verotoxin (1BOS), and *Lyophyllum decastes* fungal lectin (4NDV) show different combining site architectures. As previously suggested, the galabiose-binding adhesin SadP from Gram-positive and *E. coli* P fimbrial adhesins from Gram-negative bacteria are an example of convergent evolution toward binding to the galabiose oligosaccharide. The structural similarities thus confirm this hypothesis.

Hemagglutination positive strains expressing type P_N SadP from pig and zoonotic meningitis strains belong to serotype 2 and clonal group CC1 (6, 17). *S. suis* hemagglutination type P_O strains were mostly found from serotype 4 and were isolated from lungs of strains causing pneumonia (28). The majority of strains that have the gene encoding type P_N SadP belong to a distinct population consisting of systemic isolates, which were identified in a large BRaTP1T consortium functional genomic study (12). *S. suis* strains that cause human meningitis comprise a separate clade and are thought to have evolved when pig farming was intensified in 1920s (12). Zoonotic *S. suis* strains as a specific population have been thought to exponentially spread to different geographical areas due to the selection of pigs that are optimal in terms of productivity. The BRaTP1T consortium study of *S. suis* genomic signatures for pig and human infections has suggested that the systemic infections are genetically

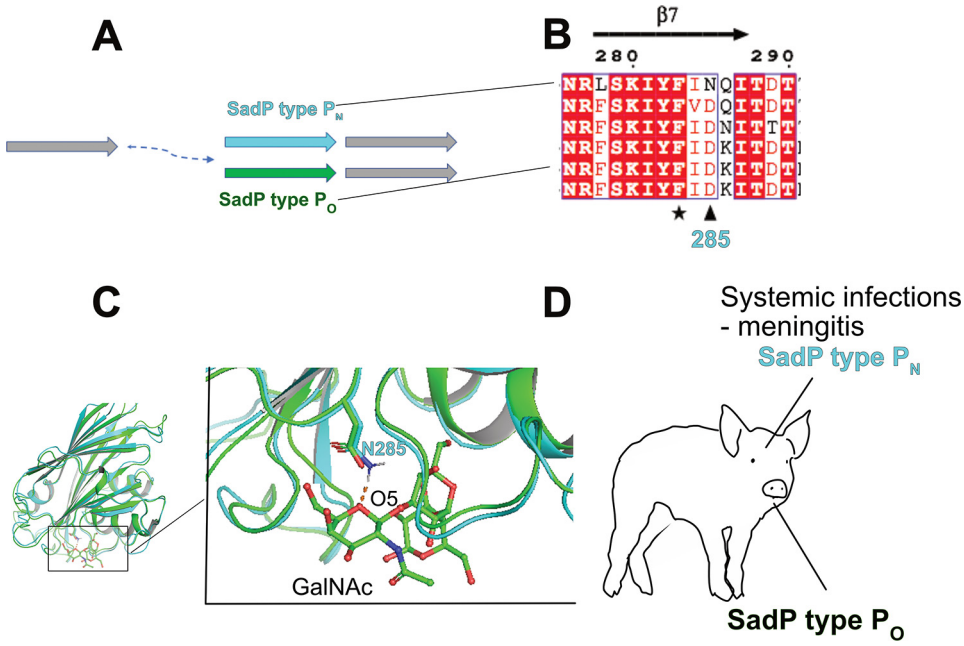

Figure 9. Summary of the results. *A,* SadP-type P_N (*cyan*) and type P_O (*green*) are putative duplicates of the downstream SadP homolog (*gray*). *B,* conservative change of type P_N SadP asparagine 285 to aspartic acid of SadP-type P_O. *C,* this study has shown the mechanism how Asn-285 contributes to the binding of terminal GalNAcβ1-saccharide of Gb4 by a specific interaction with GalNAc hexose ring oxygen (*orange dashed line*). The 3D structure of the SadP-type P_O from type 4 *S. suis* 6407 was obtained by homology modeling (Swiss Prot) and superimposed structures of type P_N (*cyan*) in complex with GalNAcβ1–Galα1–4Gal and type P_O (*green*) were created with PyMOL. The structures suggest that the abolishment of Gb4 binding is based on the same mechanism as shown with the N285D mutant. *D,* the results of the binding mechanisms of SadP-type P_N with Gb4 and the distribution of SadP subtypes in *S. suis* clinical and nonclinical strains suggest that SadP Gb4 binding is associated with strains causing systemic disease. Therefore, the molecular mechanism of SadP-type P_N binding to Gb4 could be targeted to prevent *S. suis* systemic diseases.

determined and the genome size of highly virulent strains is reduced and enriched with virulence genes. Because the type P_N SadP adhesin gene has not been lost in strains causing systemic infections, it is tempting to speculate that the recognition of Gb4 may play a specific role in invasive infections. In a previous study, type P_N SadP (designated SadP1) present in CC1 clonal group of *S. suis* strains (17) was found to specifically adhere better to human intestinal cells (Caco-2) than to pig intestinal cells. This could indicate that type P_N SadP has specific binding preferences to human intestine, thus promoting zoonosis.

In summary, the results of the present study could have implications toward the therapeutic applications targeting SadP and *S. suis* systemic infections (Fig. 9). The gene encoding SadP-type P_N has a downstream homolog, which is a pseudogene (has a stop codon). It could be speculated that the gene encoding SadP-type P_N is a putatively duplicated gene, which has evolved to bind Gb4 (Fig. 9*A*). This study shows the molecular mechanism how Asn-285 contributes to the binding of terminal GalNAcβ1-saccharide of Gb4 by a specific interaction with GalNAc hexose ring oxygen (Fig. 9, *B* and *C*). The analogous Asn-285–mediated binding mechanisms to Gb4 and glycomimetic phenylurea-galabiose could be utilized in the design of therapeutics against the invasive systemic infections without disturbing the commensal *S. suis* bacteria colonizing pig upper respiratory tract.

Experimental procedures

Bacterial strains

The chromosomal DNA of type P_N and P_O *S. suis* strains (6) was purified using GelElute bacterial genomic DNA kit according to the manufacturer's instructions. *Streptococci* were grown in Todd-Hewitt broth supplemented with 0.5% yeast extract or in Columbia agar plates supplemented with 5% sheep blood in 5% CO_2 at 37 °C and *E. coli* strains were grown in LB medium. Antibiotics used were 30 μg/ml of kanamycin (pET28) and 100 μg/ml of ampicillin (pET46EkLIC) in *E. coli* and 500 μg/ml of kanamycin for *S. suis* D282Δ*SadP* mutant (6). *Escherichia coli* NovaBlue (Novagen) was used for the cloning of SadP constructs and strain BL21(DE3) for expression of the adhesin.

Cloning and construction of recombinant adhesins

The galabiose-binding N-terminal domains of SadP from hemagglutination subtypes P_N (serotype 2 strain D282) and P_O (serotype 4 strains 752, 825, and 6407, serotype 1 strain 836, and nontypeable strain B147) were cloned into pET46EkLIC vector as follows. The primer pairs SadPDER48 (gacgacgacaagatagaatcgctagaaccagatgtt) and SadPDER49 (gaggagaagcccggttattcttctcaagggtaatctc) were designed to clone the 882-bp fragment of the adhesin N-terminal galabiose-binding domain. The fragments were amplified with Phusion HotStart II DNA polymerase and were cloned into LIC-vector (LIC, ligation independent cloning) pET46EkLIC (Novagen). The ligation products were transformed into NovaBlue-competent cells. This construct yielded a 33.4-kDa His_6-tagged fusion protein (SadP (31-328)). The sequence of N-terminal domains of SadP homologs were verified by sequencing with T7 promoter and T7 terminator primers. The vectors were transformed into expression strain BL21(DE3).

Site-specific mutant to type P_N SadP(31-328) W258A was constructed by PCR with 5′-phosphorylated forward primer tgg aac gca tct gct ggt caa gct and reverse primer ttg aga att aaa acc att ttc. The PCR product was amplified with Phusion Hot-Start II DNA polymerase and the PCR fragment was ligated with T4 ligase (Promega) and transformed into NovaBlue competent cells. The resulting plasmid SadP(31-328)W258A-pET28a was sequenced to verify the mutation.

Synthetic gene construct and the corresponding site-specific mutants for WT SadP(125-328) type P_N were obtained from GenScript. Site-specific mutants constructed were Δ244-246 (PSAD-1), N285D (PSAD-2), E292Q (PSAD-3), N285D/Δ244-246 (PSAD-4), and H216-D246delinsDELFNRFPNKVDSTNNGDGAPFRFFNKE (PSAD-5) (replacement of aa 216-242 into corresponding sequence of type P_O of strain 6107).

Bioinformatics

To compare the distribution of SadP alleles in *S. suis* from different infections, *e.g.* invasive, respiratory, and nonclinical samples, the presence of either P_N or P_O alleles were detected from 374 previously published *S. suis* isolates (12) using SRST2 software version 0.2.0 with default settings (29). The SadP genes from *S. suis* P1/7 (AM946016.1) and 6407 (NZ_CP008921.1) were used as reference sequences for P_N and P_O, respectively. The distribution of P_N and P_O alleles in the *S. suis* phylogeny was investigated by creating a core-genome maximum-likelihood tree using Roary version 3.12.0 (30) and RAxML version 8.2.8 (31) from the 374 isolates.

Expression and purification of SadP proteins

The bacteria were grown at 30 °C, 250 rpm, to an A_{600} of 0.5, and the protein expression was induced with 0.2 mM isopropyl 1-thio-β-D-galactopyranoside for 3.5 h. Bacteria were harvested by centrifugation with 3000 × *g*, at +4 °C and stored at −84 °C. The recombinant protein was purified with Ni-NTA affinity chromatography. Briefly, bacteria were lysed with 0.4 mg/ml of hen egg lysozyme (Sigma) in 50 mM sodium phosphate buffer, pH 8.0, containing 0.5 M NaCl, EDTA-free protease inhibitor mixture (Pierce), 20 mM imidazole, 20 μg/ml of DNase, and 1 mM $MgCl_2$ on ice for 30 min. The lysate was sonicated to further homogenize the cell debris and centrifuged at 20,000 × *g*, +4 °C for 30 min. The filtered lysate was purified with Ni-NTA affinity chromatography using HiPrep FF column connected to Äktaprime Plus, GE Healthcare, at +25°C. Further purification was done with a gel filtration HiLoad 16/60 Superdex 200 column using Tris-HCl, pH 7.5, 0.15 M NaCl as running buffer. The purity of the recombinant proteins was analyzed with SDS-PAGE chromatography.

Crystallization

SadP N285D mutant (15 mg/ml) was crystallized with the hanging drop vapor-diffusion method. The well condition contained 1.3-1.5 M sodium citrate tribasic, 0.1 M sodium cacodylate, pH 6.5. Equal volumes of well solution and protein (2 μl + 2 μl) were mixed and the crystals grew at 16 °C, initially as haystacks of very thin needles. Single crystals suitable for data collection were subsequently grown by using the seeding technique. A small part of the haystack was crushed with a metallic needle in the crystallization drop and 0.2 μl were diluted in 20 μl of mother liquor to create a seeding stock. Pre-equilibrated (1 day old) crystallization drops were seeded with 0.1 μl of the seeding stock. Single crystals started to grow after ∼3 days.

Data collection and crystal structure determination and refinement

Diffraction data were collected on the BioMAX beamline at MAX IV (Lund, Sweden) from a single crystal under cryogenic temperatures (100 K). The crystal diffracted to 1.85 Å but the resolution was later truncated during processing to 2.05 Å because of completeness. The crystal was found to belong to the *C*2 space group. Data processing was carried out with automated procedures in EDNA (32) and scaling was done with AIMLESS (33).

Molecular replacement with PHASER (34) was carried out to obtain initial phases using the native structure as a template. Five molecules in the crystallographic asymmetric unit were located (Matthews coefficient 2.67 $Å^3$/Da corresponding to ∼53.9% solvent content). Initial building of the structure was carried out using the automated building procedure in BUCCANEER (35) using the ccp4i2 interface (36). After the initial building that produced an almost complete structure, the refinement continued in PHENIX v.1.17.1-3660 (37) using simulated annealing at 1000 K with maximum likelihood as target function. The first round of simulated annealing resulted in R_{work}/R_{free} of 0.227/0.269. Inclusion of waters and rounds of manual rebuilding using COOT (38) alternated with PHENIX refinement resulted in the final structure with R_{work}/R_{free} of 0.174/0.221 (Table S1). A glycerol molecule was found bound in each of the A, C, and D subunits. Two glycerol molecules were located in the binding site of subunit B.

Isolation of SadP-binding glycosphingolipids from porcine lung

Nonacid glycosphingolipids were isolated from porcine lung as described (39). Briefly, the lung tissue was lyophilized, and then extracted in two steps in a Soxhlet apparatus with chloroform/methanol (2:1 and 1:9, by volume, respectively). The material obtained was subjected to mild alkaline hydrolysis and dialysis, followed by separation on a silicic acid column. Acid and nonacid glycosphingolipid fractions were obtained by chromatography on a DEAE-cellulose column. To separate the nonacid glycolipids from alkali-stable phospholipids, this fraction was acetylated and separated on a second silicic acid column, followed by deacetylation and dialysis. Final purifications were done by chromatographies on DEAE-cellulose and silicic acid columns.

The total nonacid glycosphingolipid fraction (9 mg) from porcine lung was first separated on an Iatrobeads (Iatrobeads 6RS-8060; Iatron Laboratories, Tokyo) column (1.0 g) and eluted with increasing volumes of methanol in chloroform. Aliquots of the fractions obtained were analyzed by TLC. Fractions that were colored green by anisaldehyde were tested for binding of SadP using the chromatogram-binding assay. SadP

bound to a fraction containing glycosphingolipids migrating in the tri- and tetraglycosylceramide regions on thin-layer chromatograms. This fraction (1.0 mg) was further separated on an Iatrobeads column (1.0 g), eluted with chloroform/methanol/water, 65:25:4 (by volume), 30 × 0.5 ml, followed by chloroform/methanol/water, 65:25:4, for 10 min. The SadP-binding triglycosylceramide was eluted in fractions 12-17, and these fractions were pooled into one fraction migrating as a single band (0.2 mg, denoted fraction PL-1), and fraction migrating as a double band (0.3 mg, denoted fraction PL-2) on thin-layer chromatograms. In addition, a SadP tetraglycosylceramide was present in fractions 19-31, and pooling of these fractions gave 0.4 mg (denoted fraction PL-4).

Reference glycosphingolipids

Total acid and nonacid glycosphingolipid fractions were isolated as described (39), and the individual glycosphingolipids were obtained by repeated chromatography on silicic acid columns, and by HPLC, and identified by MS (20, 40) and ^{1}H NMR spectroscopy (41).

Thin-layer chromatography

Aluminum- or glass-backed Silica Gel 60 high performance TLC plates (Merck, Darmstadt, Germany) were used for TLC, and chromatographed with chloroform/methanol/water (60:35:8 by volume) as solvent system. The different glycosphingolipids were applied to the plates in quantities of 4 μg of pure glycosphingolipids, and 20-40 μg of glycosphingolipid mixtures. Chemical detection was done with anisaldehyde (42).

Radiolabeling

Aliquots of 100 μg of the different SadP protein preparations were labeled with ^{125}I by the Iodogen method according to the manufacturer's instructions (Pierce/Thermo Scientific), giving ~2000 cpm/μg of protein.

Chromatogram-binding assays

Binding of radiolabeled proteins to glycosphingolipids on thin-layer chromatograms was done as described (43). Chromatograms with separated glycosphingolipids were dipped for 1 min in diethylether/*n*-hexane (1:5, by volume) containing 0.5% (w/v) polyisobutylmethacrylate (Aldrich). After drying, the chromatograms were soaked in PBS containing 2% (w/v) BSA, 0.1% (w/v) NaN_3, and 0.1% (w/v) Tween 20 (Solution A), for 2 h at room temperature. Thereafter the plates were incubated with ^{125}Ilabeled SadP protein (1-5 × 10^6 cpm/ml) for 2 h at room temperature. After washing six times with PBS, and drying, the thin-layer plates were autoradiographed for 12 h using XAR-5 Xray films (Eastman Kodak).

Microtiter well assay

Binding of radiolabeled SadP to glycosphingolipids in microtiter wells was performed as described (43). In short, 250 μg of pure glycosphingolipids in methanol were applied to microtiter wells (Falcon 3911, Becton Dickinson Labware). When the solvent had evaporated, the wells were blocked for 2 h at room temperature with 200 μl of BSA/PBS. Thereafter, the wells were incubated for 4 h at room temperature with 50 μl of ^{125}I-labeled SadP (2 × 10^3 cpm/μl) diluted in BSA/PBS. After washing 6 times with PBS, the wells were cut out and the radioactivity was counted in a γ counter.

LC-ESI/MS of native glycosphingolipids

Native glycosphingolipids were analyzed by LC-ESI/MS as described (44). Glycosphingolipids were dissolved in methanol/acetonitrile at 75:25 (by volume) and separated on a 200 × 0.150-mm column, packed in-house with 5 μm polyamine II particles (YMC Europe GmbH, Dinslaken, Germany). An autosampler, HTC-PAL (CTC Analytics AG, Zwingen, Switzerland) equipped with a cheminert valve (0.25 mm bore) and a 2-μl loop were used for sample injection. An Agilent 1100 binary pump (Agilent Technologies, Palo Alto, CA) delivered a flow of 250 μl/min, which was split down in an 1/16 inch microvolume-T (0.15 mm bore) (Vici AG International, Schenkon, Switzerland) by a 50 cm × 50 μM inner diameter fused silica capillary before the injector of the autosampler, allowing ~2-3 μl/min through the column. Samples were eluted with an aqueous gradient (A: 100% acetonitrile, to B: 10 mM ammonium bicarbonate). The gradient (0–50% B) was eluted for 40 min, followed by a wash step with 100% B, and equilibration of the column for 20 min. The samples were analyzed in negative ion mode on a LTQ linear quadropole ion trap mass spectrometer (Thermo Electron, San José, CA), with an IonMax standard ESI source equipped with a stainless steel needle kept at −3.5 kV. Compressed air was used as nebulizer gas. The heated capillary was kept at 270 °C, and the capillary voltage was –50 kV. Full scan (*m/z* 500-1800, two microscans, maximum 100 ms, target value of 30,000) was performed, followed by data-dependent MS^2 scans (two microscans, maximum 100 ms, target value of 30,000) with normalized collision energy of 35%, isolation window of 2.5 units, activation q = 0.25, and activation time 30 ms). The threshold for MS^2 was set to 500 counts. Data acquisition and processing were conducted with Xcalibur software version 2.0.7 (Thermo Fisher Scientific). Manual assignment of glycosphingolipid sequences was done with the assistance of the Glycoworkbench tool (version 2.1), and comparison of retention times and MS^2 spectra of reference glycosphingolipids.

Endoglycoceramidase digestion and LC-ESI/MS

Endoglycoceramidase II from *Rhodococcus* spp. (Ito) (Takara Bio Europe S.A., Gennevilliers, France) was used for hydrolysis of glycosphingolipids. Briefly, 50 μg of glycosphingolipids were resuspended in 100 μl of 0.05 M sodium acetate buffer, pH 5.0, containing 120 μg of sodium cholate, and sonicated briefly. Thereafter, 1 milliunit of enzyme was added, and the mixture was incubated at 37 °C for 48 h. The reaction was stopped by addition of chloroform/methanol/water to the final proportions, 8:4:3 (by volume). The oligosaccharide-containing upper phase thus obtained was separated from detergent on a Sep-Pak QMA cartridge (Waters). The eluant containing the oligosaccharides was dried under nitrogen and under vacuum.

The glycosphingolipid-derived oligosaccharides were resuspended in 50 μl of water and analyzed by LC-ESI/MS as

described (20). The oligosaccharides were separated on a column (200 × 0.180 mm) packed in-house with 5-μm porous graphite particles (Hypercarb, Thermo-Hypersil, Runcorn, UK). An autosampler, HTC-PAL (CTC Analytics AG, Zwingen, Switzerland) equipped with a cheminert valve (0.25 mm bore) and a 2-µl loop were used for sample injection. An Agilent 1100 binary pump (Agilent Technologies, Palo Alto, CA) delivered a flow of 250 µl/min, which was split down in an 1/16 inch microvolume-T (0.15 mm bore) (Vici AG International, Schenkon, Switzerland) by a 50 cm × 50-μm inner diameter fused silica capillary before the injector of the autosampler, allowing ~2-3 µl/min through the column. The oligosaccharides (3 µl) were injected onto the column and eluted with an acetonitrile gradient (A: 10 mM ammonium bicarbonate; B: 10 mM ammonium bicarbonate in 80% acetonitrile). The gradient (0–45% B) was eluted for 46 min, followed by a wash step with 100% B, and equilibration of the column for 24 min. A 30 cm × 50-μm inner diameter fused silica capillary was used as transfer line to the ion source.

The oligosaccharides were analyzed in negative ion mode on an LTQ linear quadrupole ion trap mass spectrometer (Thermo Electron, San José, CA). The IonMax standard ESI source on the LTQ mass spectrometer was equipped with a stainless steel needle kept at –3.5 kV. Compressed air was used as nebulizer gas. The heated capillary was kept at 270 °C, and the capillary voltage was –50 kV. Full-scan (*m/z* 380-2,000, 2 microscans, maximum 100 ms, target value of 30,000) was performed, followed by data-dependent MS^2 scans of the three most abundant ions in each scan (2 microscans, maximum 100 ms, target value of 10,000). The threshold for MS^2 was set to 500 counts. Normalized collision energy was 35%, and an isolation window of 3 μm, an activation q = 0.25, and an activation time of 30 ms was used. Data acquisition and processing were conducted with Xcalibur software (version 2.0.7).

Manual assignment of glycan sequences was done on the basis of knowledge of mammalian biosynthetic pathways, with the assistance of the Glycoworkbench tool (Version 2.1), and by comparison of retention times and MS^2 spectra of oligosaccharides from reference glycosphingolipids (20).

S. suis cell-binding assay

EA.hy926 cells were maintained and grown in DMEM, 10% fetal calf serum medium at 37 °C, 5% CO_2. For bacterial binding assay the cells were detached with trypsin-EDTA, counted, and 15,000 cells/well added into round glass coverslips in 24-well–plates. Cells were grown for 24-48 h to subconfluence.

S. suis D282 WT-type P_N strain and D282-Δ*sadP* were grown in THY overnight at 37 °C, 5% CO_2. Bacteria were diluted 1/20 into prewarmed 37 °C THY and grown to OD_{550} of 0.2 and diluted 1/100 into prewarmed DMEM, 10% fetal calf serum without antibiotics. 500 µl of bacterial dilution was pipetted into the wells (multiplicity of infection 100:1) and the plate was centrifuged with 800 × *g*, 15 min at 20 °C.

The plate was incubated at 37 °C for 1 h. The wells were washed 4 × 1000 µl of PBS. The cells were stained with Diff-Quick kit, washed, and the coverslips were mounted on glass slides with Permount.

The bacterial binding was quantitated by microscopy with -×100 objective with immersion oil. The bound bacteria were enumerated by counting two wells for each sample. The results were expressed as average of bacteria/optical field.

For flow cytometry, N-terminal domain of type P_N SadP(31-328) was labeled with FITC (Sigma-Aldrich) in 0.2 M borate buffer, pH 8.0, 0.16 M NaCl (50:1 molar ratio of FITC/SadP, 83 nmol of SadP, and 1.7 µmol of FITC) and the labeling was stopped with Tris buffer. The labeled SadP was purified from the free FITC with PD-10 (GE Healthcare) desalting column. The EA.hy926 cells were seeded into 6-well culture dishes (1×10^5 cells/well) and grown for 48 h. The cells were washed with DMEM and incubated with 400 ng/ml of labeled SadP with or without 10 µg/ml of pigeon ovomucoid. After binding, the wells were washed with PBS (0.15 M NaCl, 2.7 mM KCl, 8.1 mM Na_2HPO_4, 1.5 mM KH_2PO_4) and fixed with 2% (w/v) paraformaldehyde in PBS for 15 min. The cells were washed twice with PBS, and the cells were scraped of the wells and suspended into the PBS. 10,000 cells were analyzed for SadP binding with FACSCalibur.

Amplified luminescent proximity homogeneous assay (AlphaScreen)

The AlphaScreen assay was optimized as described before (19). Briefly, the assay was performed using AlphaScreen streptavidin donor beads and Ni-NTA acceptor beads (PerkinElmer Life Sciences). The molar concentrations of galabiose-containing biotinylated ovomucoid (receptor) and adhesin were optimized by finding the hook point for the interaction by setting up a matrix of proteins in 96-well AlphaPlates (PerkinElmer) in 10 mM Tris-HCl, pH 7.5, 0.15 M NaCl, 0.2% BSA, 0.05% Tween 20 0.2% (TBST, 0.2% BSA). For the optimized assay dilutions of 5 µl of the His-tagged adhesin and 5 µl of biotinylated ovomucoid were pipetted into the wells and the plates were centrifuged for 1 min, 1000 × *g*. The plates were incubated at +25 °C for 1 h. This was followed by addition of Ni-NTA beads (20 µg/ml) and incubation for 1.5 h. Finally, streptavidin donor beads were added (20 µg/ml) and the mixtures were incubated for 30 min and then measured with the Ensight multimode reader (PerkinElmer) using an excitation wavelength of 680 nm with donor beads and measurement of emission wavelength of 615 nm from AlphaLISA anti-HIS acceptor beads. For inhibition assays the oligosaccharides, whose structures have been described before (25) or depicted in Fig. 4 for TMSEt-glycosides of GalNAcβ1–3Galα1–4Gal and 3Galα1–4Gal (Fig. S8), were diluted into TBST, 0.2% BSA buffer and mixed with the His-tagged adhesin and biotinylated ovomucoid. The binding was measured as described above. The binding inhibition data were fitted using Prism with settings of log(inhibitor) *versus* response slope (four parameters).

Isothermal titration calorimetry

SadP-D282(31-328) (P_N), SadP-6107(31-328) (P_O), SadP (125-329) type P_N, and site-specific mutant SadP(125-328) N285D were desalted into PBS using PD-10 desalting column (GE Healtcare). The synthetic oligosaccharides were diluted to the same buffer. 0.1-0.2 μM SadP proteins in a 350-µl vessel

were titrated with 1.5-2 mM solutions of galabiose oligosaccharides using MicroCal (Malvern). The protein solution was stirred with 750 rpm at 25 °C and 16 injections of a volume of 2.49 μl were injected at 180-s intervals. The data from single determinations were analyzed with Origin.

Preparation of liposomes and SadP-binding assay

Vesicles were prepared as described before (45). Briefly, POPC (1-palmitoyl-2-oleoyl-glycero-3-phosphocholine, Avanti Polar Lipids), cholesterol, and glycolipids were dissolved and mixed into chloroform/methanol (2:1, v/v) containing 30% cholesterol and 2 mM glycolipids. The solvent was evaporated and the lipid film was suspended for 30 min at 60 °C in 10 mM Tris-Cl, 140 mM NaCl buffer. The lipid-buffer suspension was briefly vortexed followed by the extrusion procedure (Avanti mini extruder using 0.1-μm polycarbonate membranes filter (Avanti Polar Lipids, Alabaster, AL)) to form large unilamellar vesicles.

PVDF membrane was wetted (wetting in 100% MeOH, washing 4 × 5 min MilliQ water) and overlaid onto wet Whatman filter paper. Liposomes were serially diluted 1:10 into TBS and 2 μl of liposomes containing 2, 0.2, and 0.02 mM glycolipid was pipetted onto the membrane and the membrane was not allowed to dry during the pipetting. The membrane was saturated with 2% BSA (w/v) in TBS for 1 h at 20 °C and incubated with 10 μg/ml of recombinant SadP for 2 h at 20 °C. The membrane was washed 4 × 5 min with TBS and the bound SadP was detected with 1:10,000 dilution of anti-His primary antibody (Sigma) and 1:20,000 dilution of horseradish peroxidase-labeled secondary rabbit anti-mouse antibody (DakoCytomation). The membrane was incubated with ECL substrate (WesternBright Quantum, Labtech) and the SadP binding was imaged with Fuji LAS-4000.

STD-NMR

STD-NMR measurements were carried out on a Bruker AVANCE III HD spectrometer (Bruker BioSpin GmbH, Rheinstetten, Germany) operating at 600.13 MHz, equipped with a nitrogen-cooled triple-channel TCI inverse CryoProbe^{TM}. The pulse sequence used for the experiments was the stddiffesgp provided by Bruker. A 1× PBS buffer with a pH of 7.45 with 10% D_2O, containing 50 μM protein and 2500 μM Gb3 trisaccharide was used for the experiments. The on-resonance pulse was set to the methyl groups at 0.9 ppm and the off-resonance pulse was set at 20 ppm. A saturation time of 2 s was used and the experiments were carried out at 313 K to somewhat improve the weak signals, likely resulting from slow k_{off}. A blank experiment with only Gb3 and no protein was done to rule out any self-STD.

Molecular dynamics simulations

Molecular dynamics simulations were performed with the OPLS3 force field in Desmond (Schrödinger release 2019-4: Desmond Molecular Dynamics System, D. E. Shaw Research, New York; Maestro-Desmond Interoperability Tools, Schrödinger, New York) using default settings except for the length of the simulation. Simulations were performed with periodic boundary conditions using orthorhombic simulation boxes with SPC water model. Counterions were used to neutralize each other. Starting conformations of ligands in complex with SadP (PDB code 5BOA) were built by manually placing ligand galabiose residues in an identical position to that in the crystal structure (PDB code 5BOA). Complexes with the mutants were generated by exchanging Asn-285 for Asp-285. The complexes were then subjected to 100-ns molecular dynamics simulations. The complex of the phenylurea derivative with the N285D mutant was not stable during the 100-ns simulations. Therefore, light constraints (1 kcal mol^{-1} Å^{-1}) on the protein secondary structures were applied. Molecular images were generated using PyMOL version 2.30 (Schrodinger LLC).

Data availability

The structure presented in this paper has been deposited to the Protein Data Bank with the following accession code 6YRO. Bioinformatics data have been made publicly available and can be found at the following site: https://microreact.org/project/4RhDg4qJP.

Acknowledgments—The synthetic glycolipid Galα1–4Galβ1–*O*-bis-(SO_2-$C_{16}H_{33}$)$_2$ was a kind gift from Professor Göran Magnusson, Lund University, Sweden. A. C. P. thanks Noushin Madani for help during crystallographic data collection. S. H. thanks Aki Stubb for helping in the purification of recombinant SadP proteins. Access to MAX IV was financially assisted by iNEXT, project number 653706, funded by the Horizon 2020 programme of the European Union.

Author contributions—M. M. J., E. B., A. C. P., U. J. N., S. T., and S. H. investigation; M. M. J., E. B., A. C. P., A. P. S., J. R., T. K., U. J. N., S. M., T. K. N., J. K., J. C., R. L., S. T., and S. H. methodology; A. C. P. and A. P. S. visualization; A. C. P., J. C., S. T., and S. H. writing-review and editing; U. J. N., J. F., S. T., and S. H. conceptualization; J. F. resources; J. F., S. T., and S. H. funding acquisition; S. T. supervision; S. T. and S. H. writing-original draft.

Funding and additional information—This work was supported by Infrastructure support from the Biocenter Finland, ERC Grant 742158 (to T. K. and J. C.), Magnus Ehrnrooth Foundation Grant 2600253011 (to S. H. and J. F.), Turku University Foundation Grant 8127 (to S. H.), Swedish Cancer Foundation Grant 18 0760 (to S. T.), and governmental grants to the Sahlgrenska University Hospital.

Conflict of interest—The authors declare that they have no conflicts of interest with the contents of this article.

Abbreviations—The abbreviations used are: aa, amino acid(s); TMSEt, 2-trimethylsilylethyl)glycosides; POPC, 1-palmitoyl-2-oleoyl-glycero-3-phosphocholine; PVDF, polyvinylidene difluoride; RMSD, root mean square deviation; LIC, ligation independent cloning; PDB, Protein Data Bank; Ni-NTA, nickel-nitrilotriacetic acid; DMEM, Dulbecco's modified Eagle's medium; ESI, electrospray ionization.

References

1. Pizarro-Cerdá, J., and Cossart, P. (2006) Bacterial adhesion and entry into host cells. *Cell* **124,** 715–727 CrossRef Medline
2. Weinbaum, S., Tarbell, J. M., and Damiano, E. R. (2007) The structure and function of the endothelial glycocalyx layer. *Annu. Rev. Biomed. Eng.* **9,** 121–167 CrossRef Medline
3. Lingwood, C. A., Binnington, B., Manis, A., and Branch, D. R. (2010) Globotriaosyl ceramide receptor function: where membrane structure and pathology intersect. *FEBS Lett.* **584,** 1879–1886 CrossRef Medline
4. Strömberg, N., Marklund, B. I., Lund, B., Ilver, D., Hamers, A., Gaastra, W., Karlsson, K. A., and Normark, S. (1990) Host-specificity of uropathogenic *Escherichia coli* depends on differences in binding specificity to Galα1-4Gal-containing isoreceptors. *EMBO J.* **9,** 2001–2010 CrossRef Medline
5. Chemani, C., Imberty, A., de Bentzmann, S., Pierre, M., Wimmerova, M., Guery, B. P., and Faure, K. (2009) Role of LecA and LecB lectins in *Pseudomonas aeruginosa*-induced lung injury and effect of carbohydrate ligands. *Infect. Immun.* **77,** 2065–2075 CrossRef Medline
6. Kouki, A., Haataja, S., Loimaranta, V., Pulliainen, A. T., Nilsson, U. J., and Finne, J. (2011) Identification of a novel streptococcal adhesin P (SadP) protein recognizing galactosyl-α1-4-galactose-containing glycoconjugates: convergent evolution of bacterial pathogens to binding of the same host receptor. *J. Biol. Chem.* **286,** 38854–38864 CrossRef Medline
7. Rello, J., Parisella, F. R., and Perez, A. (2019) Alternatives to antibiotics in an era of difficult-to-treat resistance: new insights. *Expert Rev. Clin. Pharmacol.* **12,** 635–642 CrossRef
8. Alves, M., Ferreira, I. F. R., Dias, J., Teixeira, V., Martins, A., and Pintado, M. (2012) A review on antimicrobial activity of mushroom (basidiomycetes) extracts and isolated compounds. *Planta Med.* **78,** 1707–1718 CrossRef
9. Bernardi, A., Jiménez-Barbero, J., Casnati, A., Castro, C., De, Darbre, T., Fieschi, F., Finne, J., Funken, H., Jaeger, K. E., Lahmann, M., Lindhorst, T. K., Marradi, M., Messner, P., Molinaro, A., Murphy, P. V., Nativi, C., *et al.* (2013) Multivalent glycoconjugates as anti-pathogenic agents. *Chem. Soc. Rev.* **42,** 4709–4727 CrossRef Medline
10. Cozens, D., and Read, R. C. (2012) Anti-adhesion methods as novel therapeutics for bacterial infections. *Expert Rev. Anti. Infect. Ther.* **10,** 1457–1468 CrossRef Medline
11. Zhang, B., Ku, X., Yu, X., Sun, Q., Wu, H., Chen, F., Zhang, X., Guo, L., Tang, X., and He, Q. (2019) Prevalence and antimicrobial susceptibilities of bacterial pathogens in Chinese pig farms from 2013 to 2017. *Sci. Rep.* **9,** 9908 CrossRef Medline
12. Weinert, L. A., Chaudhuri, R. R., Wang, J., Peters, S. E., Corander, J., Jombart, T., Baig, A., Howell, K. J., Vehkala, M., Välimäki, N., Harris, D., Chieu, T. T. B., Van Vinh Chau, N., Campbell, J., Schultsz, C., *et al.* (2015) Genomic signatures of human and animal disease in the zoonotic pathogen *Streptococcus suis*. *Nat. Commun.* **10,** 5326 CrossRef
13. Vötsch, D., Willenborg, M., Weldearegay, Y. B., and Valentin-Weigand, P. (2018) *Streptococcus suis*: the "two faces" of a pathobiont in the porcine respiratory tract. *Front. Microbiol.* **9,** 480 CrossRef Medline
14. Fittipaldi, N., Segura, M., Grenier, D., and Gottschalk, M. (2012) Virulence factors involved in the pathogenesis of the infection caused by the swine pathogen and zoonotic agent *Streptococcus suis*. *Future Microbiol.* **7,** 259–279 CrossRef Medline
15. Kouki, A., Pieters, R. J., Nilsson, U. J., Loimaranta, V., Finne, J., and Haataja, S. (2013) Bacterial adhesion of *Streptococcus suis* to host cells and its inhibition by carbohydrate ligands. *Biology (Basel)* **2,** 918–935 CrossRef Medline
16. Haataja, S., Tikkanen, K., Nilsson, U., Magnusson, G., Karlsson, K.-A. A., and Finne, J. (1994) Oligosaccharide-receptor interaction of the Galα1-4Gal binding adhesin of *Streptococcus suis*: combining site architecture and characterization of two variant adhesin specificities. *J. Biol. Chem.* **269,** 27466–27472 Medline
17. Ferrando, M. L., Willemse, N., Zaccaria, E., Pannekoek, Y., Van Der Ende, A., and Schultsz, C. (2017) Streptococcal adhesin P (SadP) contributes to *Streptococcus suis* adhesion to the human intestinal epithelium. *PLoS ONE* **12,** e0175639 CrossRef Medline
18. Kong, D., Chen, Z., Wang, J., Lv, Q., Jiang, H., Zheng, Y., Xu, M., Zhou, X., Hao, H., and Jiang, Y. (2017) Interaction of factor H-binding protein of *Streptococcus suis* with globotriaosylceramide promotes the development of meningitis. *Virulence* **8,** 1290–1303 CrossRef Medline
19. Haataja, S., Verma, P., Fu, O., Papageorgiou, A. C., Pöysti, S., Pieters, R. J., Nilsson, U. J., and Finne, J. (2018) Rationally designed chemically modified glycodendrimer inhibits *Streptococcus suis* adhesin SadP at picomolar concentrations. *Chem. A Eur. J.* **24,** 1905–1912 CrossRef
20. Karlsson, H., Halim, A., and Teneberg, S. (2010) Differentiation of glycosphingolipid-derived glycan structural isomers by liquid chromatography/mass spectrometry. *Glycobiology* **20,** 1103–1116 CrossRef Medline
21. Chai, W., Lawson, A. M., and Piskarev, V. (2002) Branching pattern and sequence analysis of underivatized oligosaccharides by combined MS/MS of singly and doubly charged molecular ions in negative-ion electrospray mass spectrometry. *J. Am. Soc. Mass Spectrom.* **13,** 670–679 CrossRef Medline
22. Robbe, C., Capon, C., Coddeville, B., and Michalski, J. C. (2004) Diagnostic ions for the rapid analysis by nano-electrospray ionization quadrupole time-of-flight mass spectrometry of *O*-glycans from human mucins. *Rapid Commun. Mass Spectrom.* **18,** 412–420 CrossRef Medline
23. Suzuki, N., Khoo, K. H., Chen, H. C., Johnson, J. R., and Lee, Y. C. (2001) Isolation and characterization of major glycoproteins of pigeon egg white: ubiquitous presence of unique *N*-glycans containing Galα1-4Gal. *J. Biol. Chem.* **276,** 23221–23229 CrossRef Medline
24. Nilsson, U., Ray, A. K., and Magnusson, G. (1994) Synthesis of the globotetraose tetrasaccharide and terminal tri- and di-saccharide fragments. *Carbohydr. Res.* **252,** 117–136 CrossRef
25. Ohlsson, J., Larsson, A., Haataja, S., Alajaaski, J., Stenlund, P., Pinkner, J. S., Hultgren, S. J., Finne, J., Kihlberg, J., and Nilsson, U. J. (2005) Structure-activity relationships of galabioside derivatives as inhibitors of *E. coli* and *S. suis* adhesins: nanomolar inhibitors of *S. suis* adhesins. *Org. Biomol. Chem.* **3,** 886–900 CrossRef Medline
26. Steil, D., Bonse, R., Meisen, I., Pohlentz, G., Vallejo, G., Karch, H., and Müthing, J. (2016) A topographical atlas of shiga toxin 2e receptor distribution in the tissues of weaned piglets. *Toxins* **8,** 357 CrossRef
27. Diswall, M., Ångström, J., Karlsson, H., Phelps, C. J., Ayares, D., Teneberg, S., and Breimer, M. E. (2010) Structural characterization of α1,3-galactosyltransferase knockout pig heart and kidney glycolipids and their reactivity with human and baboon antibodies. *Xenotransplantation* **17,** 48–60 CrossRef Medline
28. Kurl, D. N., Haataja, S., and Finne, J. (1989) Hemagglutination activities of group B, C, D, and G streptococci: demonstration of novel sugar-specific cell-binding activities in *Streptococcus suis*. *Infect. Immun.* **57,** 384–389 CrossRef Medline
29. Inouye, M., Dashnow, H., Raven, L. A., Schultz, M. B., Pope, B. J., Tomita, T., Zobel, J., and Holt, K. E. (2014) SRST2: rapid genomic surveillance for public health and hospital microbiology labs. *Genome Med.* **6,** 90 CrossRef Medline
30. Page, A. J., Cummins, C. A., Hunt, M., Wong, V. K., Reuter, S., Holden, M. T. G., Fookes, M., Falush, D., Keane, J. A., and Parkhill, J. (2015) Roary: rapid large-scale prokaryote pan genome analysis. *Bioinformatics* **31,** 3691–3693 CrossRef Medline
31. Stamatakis, A. (2014) RAxML version 8: a tool for phylogenetic analysis and post-analysis of large phylogenies. *Bioinformatics* **30,** 1312–1313 CrossRef Medline
32. Monaco, S., Gordon, E., Bowler, M. W., Delagenière, S., Guijarro, M., Spruce, D., Svensson, O., Mcsweeney, S. M., Mccarthy, A. A., Leonard, G., and Nanao, M. H. (2013) Automatic processing of macromolecular crystallography X-ray diffraction data at the ESRF. *J. Appl. Crystallogr.* **46,** 804–810 CrossRef Medline
33. Evans, P. R., and Murshudov, G. N. (2013) How good are my data and what is the resolution?. *Acta Crystallogr. Sect. D Biol. Crystallogr.* **69,** 1204–1214 CrossRef Medline
34. McCoy, A. J., Grosse-Kunstleve, R. W., Adams, P. D., Winn, M. D., Storoni, L. C., and Read, R. J. (2007) Phaser crystallographic software. *J. Appl. Crystallogr.* **40,** 658–674 CrossRef Medline

35. Cowtan, K. (2006) The Buccaneer software for automated model building: 1. tracing protein chains. *Acta Crystallogr. Sect. D Biol. Crystallogr.* **62,** 1002–1011 CrossRef Medline
36. Potterton, L., Agirre, J., Ballard, C., Cowtan, K., Dodson, E., Evans, P. R., Jenkins, H. T., Keegan, R., Krissinel, E., Stevenson, K., Lebedev, A., McNicholas, S. J., Nicholls, R. A., Noble, M., Pannu, N. S., *et al.* (2018) CCP 4i2: the new graphical user interface to the CCP 4 program suite. *Acta Crystallogr. Sect. D Struct. Biol.* **74,** 68–84 CrossRef Medline
37. Adams, P. D., Afonine, P. V., Bunkóczi, G., Chen, V. B., Davis, I. W., Echols, N., Headd, J. J., Hung, L. W., Kapral, G. J., Grosse-Kunstleve, R. W., McCoy, A. J., Moriarty, N. W., Oeffner, R., Read, R. J., Richardson, D. C., *et al.* (2010) PHENIX: a comprehensive Python-based system for macromolecular structure solution. *Acta Crystallogr. Sect. D Biol. Crystallogr.* **66,** 213–221 CrossRef Medline
38. Emsley, P., and Cowtan, K. (2004) Coot: model-building tools for molecular graphics. *Acta Crystallogr. Sect. D Biol. Crystallogr.* **60,** 2126–2132 CrossRef Medline
39. Karlsson, K. A. (1987) Preparation of total nonacid glycolipids for overlay analysis of receptors for bacteria and viruses and for other studies. *Methods Enzymol.* **138,** 212–220 CrossRef Medline
40. Samuelsson, B. E., Pimlott, W., and Karlsson, K. A. (1990) Mass spectrometry of mixtures of intact glycosphingolipids. *Methods Enzymol.* **193,** 623–646 CrossRef Medline
41. Koerner, T. A. W., Prestegard, J. H., Demou, P. C., and Yu, R. K. (1983) High-resolution proton NMR studies of gangliosides: 1. use of homonuclear two-dimensional spin-echo J-correlated spectroscopy for determination of residue composition and anomeric configurations. *Biochemistry* **22,** 2676–2687 CrossRef Medline
42. Stahl, E., *et al.* (1962) *Dünnschicht-Chromatographie* in Modern Methods of Plant Analysis (Biemann, K., ed) pp. 214–229, Springer-Verlag, Berlin
43. Jansson, L., Angström, J., Lebens, M., Imberty, A., Varrot, A., and Teneberg, S. (2010) Carbohydrate binding specificities and crystal structure of the cholera toxin-like B-subunit from *Citrobacter freundii*. *Biochimie* **92,** 482–490 CrossRef Medline
44. Johansson, M. M., Dedic, B., Lundholm, K., Branzell, F. B., Barone, A., Benktander, J., and Teneberg, S. (2015) Characterization of moose intestinal glycosphingolipids. *Glycoconj. J.* **32,** 393–412 CrossRef Medline
45. Halling, K. K., Ramstedt, B., Nyström, J. H., Slotte, J. P., and Nyholm, T. K. M. (2008) Cholesterol interactions with fluid-phase phospholipids: effect on the lateral organization of the bilayer. *Biophys. J.* **95,** 3861–3871 CrossRef Medline
46. Robert, X., and Gouet, P. (2014) Deciphering key features in protein structures with the new ENDscript server. *Nucleic Acids Res.* **42,** W320–W324 CrossRef Medline